Structural Arrangements of Isomorphic Substitutions in Smectites: Molecular Simulation of the Swelling Properties, Interlayer Structure, and Dynamics of Hydrated Cs−Montmorillonite Revisited with New Clay Models

Brice F. Ngouana W. and Andrey G. Kalinichev*

Laboratoire SUBATECH (UMR-6457), Ecole des Mines de Nantes, 44307 Nantes, France

S *Supporting Information*

ABSTRACT: Three new structural models of montmorillonite with differently distributed Al/Si and Mg/Al substitutions in the tetrahedral and octahedral clay layers are systematically developed and studied by means of MD simulations to quantify the possible effects of such substitutional disorder on the swelling behavior, the interlayer structure, and mobility of aqueous species. A very wide range of water content, from 0 to 700 mg_{water}/g_{clay} is explored to derive the swelling properties of Cs−montmorillonite. The determined layer spacing does not differ much depending on the clay model. However, at low water contents up to 1-layer hydrate (~100 mg_{water}/g_{clay}) the variation of specific locations of the tetrahedral and octahedral substitutions in the two TOT clay layers slightly but noticeably affects the total hydration energy of the system. Using atom−atom radial distribution functions and the respective atomic coordination numbers we have identified for the three clay models not only the previously observed binding sites for Cs^+ on the clay surface but also new ones that are correlated with the position of tetrahedral substitution in the structure. The mobility of Cs^+ ions and H_2O diffusion coefficients, as expected, gradually increase both with increasing water content and with increasing distance from the clay surface, but they still remain 2 to 4 times lower than the corresponding bulk values. Only small differences were observed between the three Cs−montmorillonite models, but these differences are predicted to increase in the case of higher charge density of the clay layers and/or interlayer cations.
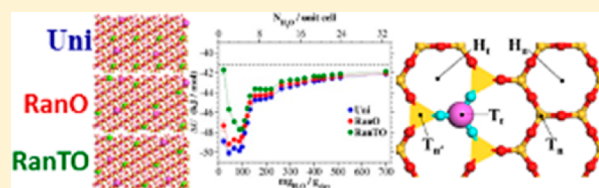
1. INTRODUCTION

Clay minerals are ubiquitous in the environment and have many properties, beneficial for their use as natural and engineered barriers in radioactive waste repositories: high sorption and ion exchange capacity, low permeability, swelling in the presence of water, etc.[1−4] Clay rocks are selected by several national programs as the preferable media for the disposal of medium- and high-level long-lived radioactive waste in deep geological formations.[5−10]

The most abundant types of clay minerals are illites (nonswelling) and smectites (swelling). Both types belong to the so-called 2:1 clay family.[11] Smectites are a major constituent of bentonite[12] used as an environmental buffer separating waste containers from a host rock formation.[13] Bentonite consists of turbostratically stacked montmorillonite layers forming individual clay particles, and a smaller fraction of accessory minerals.[14,15] Montmorillonite is also the most widespread and the most common smectite. It has a layered structure made of several stacking TOT units in which one sheet of Al-cations (O) octahedrally coordinated by oxygens and hydroxyls is sandwiched between two sheets of tetrahedrally coordinated Si-cations (T). Isomorphic substitutions (Mg for Al) and (Al for Si), in the octahedral and tetrahedral sheets, respectively, give rise to a negative clay layer charge (typically, between −0.4|e| and −1.2|e| per crystallographic unit cell[11] that is compensated

by the presence of cations in the interlayer space and on the surface of montmorillonite particles. The affinity of interlayer cations for water and the relatively weak electrostatic forces holding together montmorillonite sheets lead to an easy hydration of the charge-compensating cations in the presence of water and swelling of the clay.

The properties of cesium-containing clays have already been studied by means of both experimental[12,16−26] and molecular simulation[27−39] techniques to investigate hydration and swelling properties, interlayer and interfacial structure and dynamics of Cs^+ ions, and their preferred binding sites in montmorillonite clay. Some of these studies investigated the effect of the total clay layer charge on the above properties.[12,21,36] Onodera et al.[12] carried out experimental investigations of Cs^+ fixation in smectites. They used several clay samples with variable amounts of tetrahedral and octahedral charge in the clay layers and observed that Cs^+ sorption sites vary with the tetrahedral and octahedral charge amounts. Liu et al.[36] used three montmorillonite clay models with different amounts of total layer charge in the octahedral and tetrahedral sheets in their molecular modeling study of the thermodynamic

A

70 and structural properties of Cs—smectites. They did not find
71 significant effects of the layer charge distribution on the
72 swelling properties of Cs—smectites, but observed that layer
73 charge distribution have significant influences on the mobility
74 of interlayer Cs^{+} and preferred binding sites.

75 The contribution of computational molecular modeling to
76 our understanding of complex materials, including clays, has
77 significantly grown in recent years,[40−72] and these techniques
78 are capable to quantitatively explore their atomic-scale
79 properties not always accessible to direct experimental
80 measurements. However, more often than not, such simulations
81 are performed using relatively small structural models of clays,
82 which in combination with a relatively low layer charge
83 concentration and the application of periodic boundary
84 conditions (see section 2 below) may result in the exaggeration
85 of the actual degree of ordering in the distribution of the
86 isomorphically substituted sites in the simulated clays. Even the
87 largest simulated models of montmorillonite[73] are usually
88 constructed by simply replicating the earlier much smaller
89 structural models to the required size, so the question of the
90 effects of larger-scale disorder in the distribution of octahedral
91 and tetrahedral isomorphic substitutions on the resulting
92 properties of clays remains largely unexplored.

93 The importance of reliable understanding of the predictive
94 capabilities offered by the application of molecular modeling
95 approaches to such systems as Cs-containing clays and of the
96 present limitations of such techniques is only re-emphasized
97 with their use in the wake of the recent Fukushima accident[74]
98 when significant quantities of radioactive materials were
99 released into the environment.[75−79] Radioisotopes of cesium
100 such as the high-level ^{137}Cs contained in fission products or in
101 spent nuclear fuel were found among these materials.[80−82]
102 Cesiums isotopes (^{137}Cs, [134]Cs, and [135]Cs) are normally
103 released as nuclear waste (from nuclear power plants) in
104 which they are one of the most important sources of
105 radioactivity.[83] These radioisotopes are highly soluble[22,84] and
106 highly mobile[85] in aqueous phase. Hence in the case of their
107 accidental discharge in the environment they are likely to
108 migrate through groundwater into the biosphere[22] and have
109 very serious deleterious effects on agriculture, stock farming,
110 and, as a consequence, on human life for many years.[86]

111 The objective of our present work was to systematically
112 investigate any possible correlations between the ordering/
113 disordering in the octahedral and tetrahedral substituted sites of
114 montmorillonite (resulting in the creation of local charge
115 inhomogeneities in the clay structure) and their potential
116 effects on the swelling properties, interlayer structure, and
117 diffusion of Cs^{+} ions. For this purpose we have constructed
118 three new larger-scale montmorillonite models with the same
119 atomic composition and the same total amounts of tetrahedral
120 and octahedral charge. The only difference between the three
121 investigated models is in the degree of disorder in the
122 distribution of substituted sites in the octahedral and
123 tetrahedral sheets of the clay layer. The models were
124 constructed taking into account different possible distributions
125 of substituting structural cations in the octahedral[56,57,87−89] and
126 tetrahedral[90−92] layers of a dioctahedral smectite. Here we are
127 also taking full advantage of the capability of the CLAYFF force
128 field to more realistically represent the local charge
129 inhomogeneities formed around each specific substituted site
130 in the clay structure.[58]

131 The Cs—montmorillonite system was specifically selected for
132 this study not only because it has significant practical

133 importance but also because it has already been extensively
134 studied both experimentally and in molecular simulations.
135 Because of the particularly low charge/size ratio of the Cs^{+}
136 cation, hence its low charge density, one can expect that this
137 system should have a relatively high sensitivity to the above-
138 mentioned ordering effects. Such effects observed for the Cs—
139 montmorillonite system could exhibit themselves less strongly
140 in the case of other cations, such as Na^{+}, Ca^{2+}, or Sr^{2+}.

141 The construction of the new clay models is fully described in
142 the next section, followed by the presentation and discussion of
143 the MD simulation results obtained with these models applied
144 to the specific case of Cs—montmorillonite. Then we make
145 detailed comparisons with available experimental data and the
146 results of previous molecular modeling work for the same
147 system and formulate several general conclusions for further
148 investigation.

2. METHODOLOGY

2.1. Structural Models and Force Field Parameters.

149 The new clay models are based on a $5.16 \times 8.966 \times 9.347$ Å^3
150 pyrophyllite unit cell structure $(Si_8Al_4O_{20}(OH)_4)$ obtained by
151 single crystal X-ray refinement.[93] As in previous simula-
152 tions,[27,29,32,35,36,38,40,41,47,54,58,60,68] the clay layer of Wyom-
153 ing—montmorillonite with the chemical composition was
154 constructed by introducing the Mg/Al substitutions into one
155 out of every eight octahedral sites and Al/Si substitutions into
156 one out of every 32 tetrahedral sites. However, before
157 introducing these substitutions, the initial pyrophyllite unit
158 cell was replicated ($4 \times 4 \times 2$) along a, b, and c crystallographic
159 directions, respectively, resulting in a supercell of two TOT clay
160 layers of a total of 32 unit cells. This allowed us to prevent
161 excessive ordering of the substituted sites when the periodic
162 boundary conditions are applied.

163 Our most disordered model, corresponding to random
164 distribution of substitutions in both octahedral and tetrahedral
165 sheets is presented in Figure 1a,b. However, two less disordered
166 models were also constructed. One of them, labeled here *Uni*
167 for further discussion, corresponds to a completely uniform
168 distribution of substitutions in the octahedral sheet of the TOT
169 layer (see Figure S1a of the Supporting Information). Care was
170 taken to have at least one Al atom between two Mg/Al
171 substitutions in the a and b crystallographic directions. Then
172 Mg atomic positions of the first TOT layer were shifted in a, b,
173 and c directions to get Mg substitution positions in the second
174 TOT layer (see Figure S1b, Supporting Information). This was
175 done to avoid any symmetry of the octahedral substitution sites
176 between the two TOT layers and to ensure the proper layer
177 stacking. Since there are much fewer Al/Si tetrahedral
178 substitutions compared to the octahedral ones, they were just
179 placed in the TOT layer far from one another, not adjacent to
180 an octahedral substitution, and not at the same positions in the
181 two tetrahedral sheets of the same TOT layer. All these
182 substitutions were assigned in a manner to obey the
183 Loewenstein's rule[94] in proportion of 4 Al per 124 Si and 8
184 Mg per 56 Al in each TOT layer in order to obtain the
185 Wyoming—montmorillonite unit cell chemical composition of
186 $M^+_{0.75}(Si_{7.75}Al_{0.25})(Al_{3.5}Mg_{0.5})O_{20}(OH)_4$, where M^+ is a com-
187 pensating monovalent cation, Cs^{+} in our case.

188 Another clay model, *RanO*, corresponding to a random
189 distribution of substitutions in the octahedral sheets, was
190 obtained from the previous one by randomly changing the
191 positions of the Mg atoms in the octahedral sheets of both
192 TOT layers, while keeping the Al/Si substitutions in the
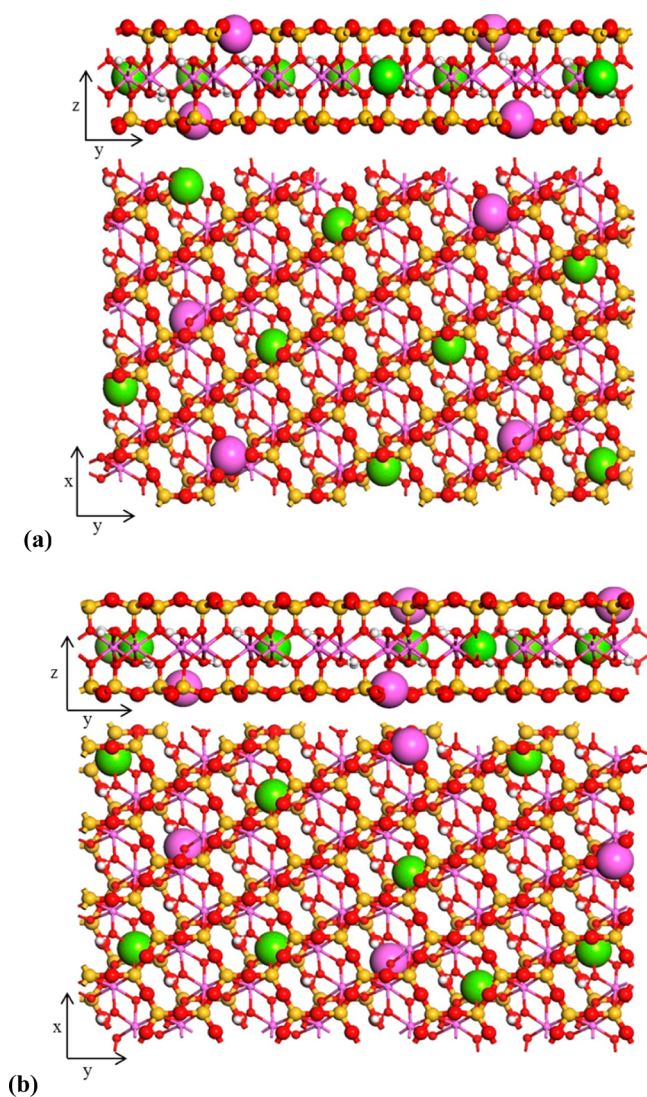
Figure 1. Side and top views of the upper (a) and lower (b) TOT layers of the most disordered clay model *RanTO*. The color code is Si (yellow), Al (pink), Mg (green), O (red), and H (white). Similar structures corresponding to the models *Uni* and *RanO* are provided in the Supporting Information.

general force field suitable for the simulation of hydrated and multicomponent mineral systems and their interfaces with aqueous solutions.[58] CLAYFF assigns partial charges of different coordinating structural oxygens taking into account, when necessary, their local coordination to the tetrahedral and/ or octahedral substituting atoms in the crystal structure[58] (see Figure 2). This force field has been proven quite successful in
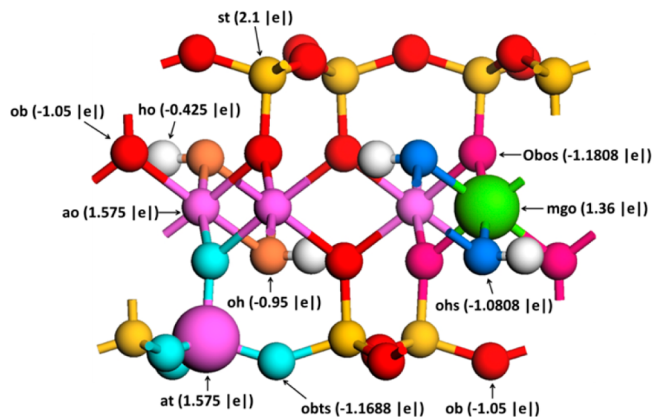
Figure 2. Schematic representation of a montmorillonite unit cell fragment with tetrahedral and octahedral substitutions and different atomic charge distributions according to CLAYFF force field.[58] O_b (bridging oxygen), O_{bts} (bridging oxygen with tetrahedral substitution), O_{bos} (bridging oxygen with octahedral substitution), O_h (hydroxyl oxygen), O_{hs} (hydroxyl oxygen with octahedral substitution), at (Al in tetrahedral coordination), ao (Al in octahedral coordination), mgo (Mg in octahedral coordination), st (Si in tetrahedral coordination).

tetrahedral sheets at the same positions (see Figure S2a,b, Supporting Information).

Finally, the clay model *RanTO*, corresponding to random distribution of substitutions in both octahedral and tetrahedral sheets, was obtained from *RanO* by keeping the octahedral substitution positions the same and randomly modifying the positions of tetrahedral substitutions in the TOT layers, while still keeping them obeying the Loewenstein's rule (see Figures 1a,b). Chávez-Páez et al.[54] used a similar approach by modifying the position of one tetrahedral substitution in two clay models.

Thus, all three clay models represented a 20.640 × 35.864 × 18.694 Å³ supercell with 90° between all the pairs of lattice vectors and identical chemical composition. All atomic positions for each of the models are provided in Tables S1–S3 of the Supporting Information.

The interatomic interactions in the model systems were described using the partial atomic charges and van der Waals parameters taken from the CLAYFF force field, a fully flexible

recent years in extensive molecular simulations of clay and clay-related materials to address a great variety of geochemical and materials science problems.[36,59,61−63,70−73,95−110] SPC water model[111] was used to represent the interactions of H_2O molecules among themselves and with the ions of the clay structure for hydrated clays and in solution.

The total energy of the systems studied is represented in CLAYFF as the sum of the contributions from the Coulombic (E_{coul}) and van der Waals (E_{vdW}) interactions of all atomic pairs and the bond stretch (E_{bond}) and angle bend (E_{ang}) interactions for the H_2O molecules and structural OH groups.[58] The van der Waals interactions are computed by means of the (12−6) Lennard-Jones potential, and the total energy can then be written as

$$E_{total} = E_{Coul} + E_{vdW} + E_{bond} + E_{ang} \tag{1}$$

with

$$E_{Coul} = \sum_{i=1}^{N_{tot}} \sum_{j=i+1}^{N_{tot}} \frac{q_i q_j}{4\pi\varepsilon_0 r_{ij}} \tag{1a}$$

$$E_{vdW} = \sum_{i=1}^{N_{tot}} \sum_{j=i+1}^{N_{tot}} 4\varepsilon_{ij} \left[\left(\frac{\sigma_{ij}}{r_{ij}} \right)^{12} - \left(\frac{\sigma_{ij}}{r_{ij}} \right)^{6} \right] \tag{1b}$$

$$E_{bond} = \frac{1}{2} \sum_{m=1}^{N_{bond}} k_m (r_m - r_{m0})^2 \tag{1c}$$

C

dx.doi.org/10.1021/jp500538z | J. Phys. Chem. C XXXX, XXX, XXX−XXX

$$E_{\text{ang}} = \frac{1}{2} \sum_{l=1}^{N_{\text{ang}}} k_l (\theta_l - \theta_{l0})^2 \tag{1d}$$

where N_{tot}, N_{bond}, and N_{ang} are the total number of atoms in the system and total number of bonded and angular terms, respectively. q_i and q_j are the partial charges of the atoms i and j, and r_{ij} is the distance between them. k_m and k_l are the harmonic force constants for bond stretching and angle bending terms for the mth bond and lth angle in the system, respectively, while r_{m0} and θ_{l0} are the equilibrium values of the corresponding bonds and angles. σ_{ij} and ε_{ij} are Lennard-Jones parameters for two interacting atoms i and j, which are obtained from the parameters of the interacting atoms by using the Lorentz−Berthelot combining rules:

$$\sigma_{ij} = \frac{1}{2} (\sigma_i + \sigma_j) \tag{2a}$$

$$\varepsilon_{ij} = (\varepsilon_i \varepsilon_j)^{1/2} \tag{2b}$$

2.2. Simulations Details. The simulated supercell contained 32 clay crystallographic unit cells and two interlayers. Three such supercells were created for each of the three clay models. Before starting the simulations the clay interlayer spaces were increased in the c direction. Then charge-compensating Cs^+ cations ions were placed at the midplane of these interlayer spaces, and water molecules were added randomly (see Figure 3). For each of the three clay models 23
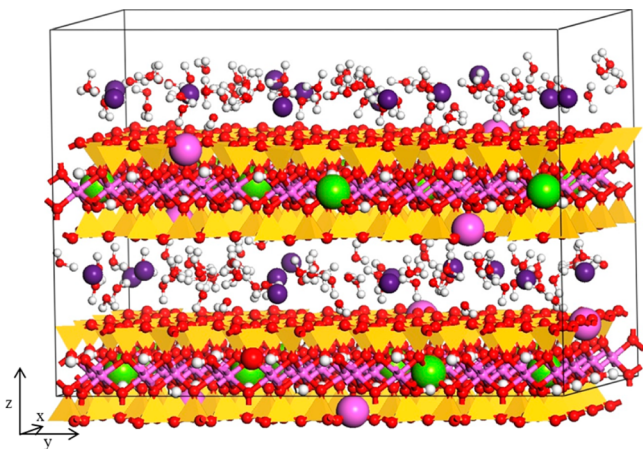
Figure 3. Snapshot of one of the simulated Cs−montmorillonite systems with water content corresponding to 6 H_2O molecules per Cs^+ ion or 5 H_2O per unit cell (1-layer hydrate).

different hydration levels were investigated in a wide range of water contents (from 0 to 700 $mg_{\text{water}}/g_{\text{clay}}$, corresponding to compositions $x = n_{\text{H2O}}/(\text{clay unit cell})$ ranging from 0 to 32). Thus, all three models at each hydration level had the same chemical composition of $Cs_{24}(Si_{248}Al_8)(Al_{112}Mg_{16})$-$O_{640}(OH)_{128} \cdot 32H_2O$. The total energy of each system for each hydration level was then minimized, allowing initial adjustments of the simulation supercell lengths.

The swelling behavior of these Cs−montmorillonite models was studied by performing 2 ns MD runs in the NPT-ensemble at $T = 298$ K and $P = 1$ bar for each of the three clay models and 23 different hydration levels. During these runs, the simulated supercell dimensions were allowed to vary independently of each other and adjust according to the water content. The last 1 ns of each trajectory was taken to compute statistical averages for a total of 10 equal blocks, to determine the supercell dimensions, the basal spacing, hydration energy, and immersion energy. These properties were computed according to the procedures described in the next subsection. Their error bars were estimated using the block averaging method[112] and presented with 95% confidence interval.

The structural and dynamical properties of Cs and water were determined for 4 different hydration levels, after 1.5 ns NVT-ensemble MD simulations at 298 K. The simulation supercells of these NVT runs were adjusted to the average equilibrium supercell dimensions obtained from the previous NPT runs for each of the 4 hydration levels. The equilibrium parts of the NVT trajectories were then analyzed to determine atomic density profiles, radial distribution functions, and diffusion coefficients of the Cs^+ ions and H_2O molecules in the hydrated clay media.

LAMMPS simulation package[113] was used for all MD runs with the integration time step of 1 fs. A spherical cut off of 10.0 Å was applied for short-range van der Waals interactions, while the long-range electrostatic interactions were treated using the Ewald summation method[114] with a precision of 10^{-4} in combination with the direct pairwise interactions calculation within a spherical cut off of 10.0 Å.

2.3. Simulation Analyses. *2.3.1. Swelling Properties.* The basal spacing as a function of water content essentially shows how the volume of the system changes with increasing (or decreasing) hydration. At the end of the NPT runs, the basal spacing (d) was calculated as follows:

$$d = \frac{\langle a \rangle \langle b \rangle \langle c \rangle}{2 \langle a \rangle \langle b \rangle} = \frac{\langle c \rangle}{2} \tag{3}$$

where $\langle a \rangle$, $\langle b \rangle$, and $\langle c \rangle$ are the statistically averaged dimensions of the simulation supercell.

In order to quantify the thermodynamics of hydration and swelling for three different Cs−montmorillonite models, we calculated the hydration energy, immersion energy,[27,36,40,41,96−98,100] and the isosteric heat of adsorption[27] at each of the hydration states.

The hydration energy (ΔU) evaluates the energy change associated with water uptake by the dry clay, and can be calculated using the generic formula:

$$\Delta U = \frac{\langle U(N) \rangle - \langle U(0) \rangle}{N} \tag{4}$$

where N is the number of interlayer water molecules for a given hydration level, while $\langle U(N) \rangle$ and $\langle U(0) \rangle$ are the average potential energies of the hydrated clay (with N water molecules) and dry clay ($N = 0$), respectively.

The immersion energy (Q) is the energy consumed or released when the clay system at a given hydration level is brought to another hydration level by adding water to the system:

$$Q = \langle U(N) \rangle - \langle U(N_0) - (N - N_0) U_{\text{bulk}} \rangle \tag{5}$$

where N_0 and $\langle U(N_0) \rangle$ are the number of water molecules and the average potential energy of a reference hydration level. U_{bulk} is the average potential energy of bulk SPC water that was computed in this work from preliminary 500 ps NVT-ensemble MD simulations of 1024 water molecules at 298 K and a water density of 0.9942 g/cm^3, following a 100 ps equilibration in the NPT-ensemble at the same temperature and pressure of 1 bar.

Considering clay at a certain hydration level, the isosteric heat of adsorption is the measure of energy released or consumed by the system when a small amount of water is added or removed from the system. This property is calculated from simulations as follows:

$$q_{st} = RT - \frac{\langle U(N) \rangle - \langle U(N') \rangle}{(N' - N)} \tag{6}$$

where N and N' are two consecutives hydration levels, R is the ideal gas constant, and T is the temperature. The factor of RT is needed for conversion between energy and enthalpy.

2.3.2. Structural and Dynamical Properties. Atom−atom radial distribution functions of the interlayer species and their atomic density profiles perpendicular to the layering were calculated to analyze the structural properties of the swelling clay. Both properties were averaged over the two statistically independent interlayer spaces and over entire trajectories from the equilibrium NVT-simulations. Density profiles, $\rho_\alpha(z)$, were determined as the average number of atoms, $\langle N_\alpha(\Delta z) \rangle$, of certain type α in a slice of thickness Δz parallel to the clay surface, normalized by the system volume, V:

$$\rho_\alpha(z) = \frac{\langle N_\alpha(\Delta z) \rangle}{V} \tag{7}$$

The coordination of atoms in clay interlayers with respect to each other (eq 9) was derived from the radial distribution function (eq 8):

$$g_{\alpha\beta}(r_{\alpha\beta}) = \frac{\langle N_{\alpha\beta} \rangle}{4\pi\rho_\beta r_{\alpha\beta}} \tag{8}$$

$$n_{\alpha\beta}(r_{\alpha\beta}) = 4\pi\rho_\beta \int_0^{r_{\alpha\beta}} g(r) r^2 dr \tag{9}$$

where $r_{\alpha\beta}$ is the distance between atoms α and β, ρ_β is the number density of atoms β, and $\langle N_{\alpha\beta} \rangle$ the average number of atoms β found at the distance $r_{\alpha\beta}$ from atom α.

The self-diffusion coefficients of interlayer species were determined from their mean squared displacement (MSD) according to the Einstein relationship:[114]

$$\frac{1}{N} \sum_{i=1}^{N} \langle |r_i(t) - r_i(t_0)|^2 \rangle = 2dDt \tag{10}$$

where N is the number of atoms of interest, $r_i(t)$ is the position of atom i at time t, and the angular brackets indicate the averaging taken over all time origins t_0 along the MD trajectory. D in eq 10 is the diffusion coefficient, and d is the dimensionality of the system equal to 1, 2, or 3 for the calculation of one-dimensional, two-dimensional, or three-dimensional diffusion coefficients, respectively.

From this equation we are then able to determine individual special components of the diffusion coefficients of interlayer species. It is known from previous simulations of clays and other layered systems[3,35,36,38,70,109] that for very long simulation times, the diffusion of aqueous species in the clay interlayers is mostly two-dimensional and occurs along the directions parallel to the clay surfaces (xx and yy). The diffusion is significantly restricted along the direction normal to the layering (zz). This was also observed in our investigated clay systems that were ran for 1 ns each. This means that the two-dimensional D_{xy} diffusion coefficient is a reasonable estimate of the diffusion of aqueous species in the interlayer spaces. However, we consider that the small value of the restricted normal component of diffusion is due to the presence of the clay layers that limit the motions of interlayer species in the considered directions, and this normal component has to be taken into account during the determination of the total diffusion coefficients for comparison with the bulk case. In particular, when comparison with experimental data is concerned, we know that these data are determined for three-dimensional diffusion.

Another important question is the comparison of diffusion coefficients in the clay interlayers with their corresponding bulk values between various experimental and simulation sources. In this case, following the previous work of Kosakowski et al.[35] and Bourg and Sposito,[70] we are using relative diffusion coefficients to minimize the uncertainties introduced by the potential inaccuracy in reproducing experimentally observed bulk diffusion coefficients by different force field models for H_2O and ions and to most directly compare the retardation or acceleration of molecular mobility in the clay interlayers with respect to the bulk solution:

$$D_r = \frac{D_{interlayer}}{D_{bulk}} \tag{11}$$

In section 3.6, we are presenting such 3D relative diffusion coefficients to compare the results obtained using our three new clay models with previous simulations and experimental data.

The MSDs used to derive the diffusion coefficients were calculated from the last 500 ps of our 1 ns equilibrium MD trajectories. A time interval of 0.5 ps was used between two consecutively saved states. The quasi-linear part of the MSDs was divided into 4 blocks. The diffusion coefficients and their statistical uncertainties were then determined by block averaging of the 4 independent MSD slopes and assuming d = 3 in eq 10. Diffusion coefficients of Cs^+ ions and H_2O molecules in bulk aqueous solution were also determined following the previously described procedure from 100 ps NPT and 500 ps NVT MD simulations of a system of 16 (Cs^+, Cl^-) pairs dissolved in 1024 water molecules using the same force field parameters as for the clay simulations. All the diffusion data from this work are shown with a $\pm 2\sigma$ confidence interval.

3. RESULTS AND DISCUSSION

3.1. Layer Spacing. Figure 4 illustrates the variation of basal layer spacing in Cs−montmorillonite as a function of water content from our simulations and provides a comparison with available experimental results.[17−19,23] There are no observable differences on the calculated layer spacing between our three clay models with different distribution of substitutions. For all three models the dry clay layer spacing of 10.60 Å is similar to the simulation (10.50−10.70 Å) and 5% lower than experimental values (11.2 Å) that are provided in Table 1. For all three clay models, a plateau corresponding to the formation of a stable monolayer hydrate is clearly observable at ∼12.6 Å, in good agreement with the range of 12.3−12.6 Å reported from experiments[17−19,23] and 12.2−12.9 Å obtained from previous simulations.[27,31,35,36] In our simulations, this monolayer hydrate corresponds to x = 4.5, which is in the range of 4.0−5.5 observed in previous simulation studies (see Table 1).

Table 1 also shows comparison between our data and other simulation results for layer spacings corresponding to stable 2-

E

dx.doi.org/10.1021/jp500538z | J. Phys. Chem. C XXXX, XXX, XXX−XXX
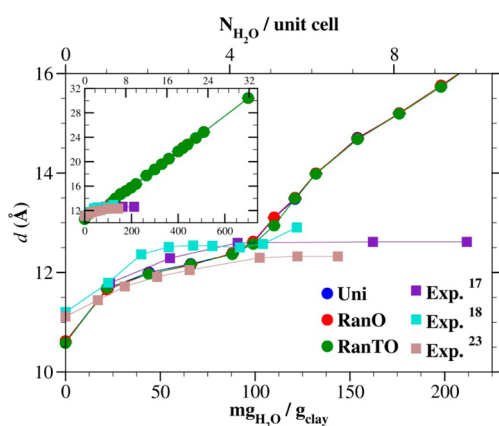
Figure 4. Swelling curves of Cs−montmorillonite simulated with three new clay models *Uni* (blue), *RanO* (red), and *RanTO* (green). Available experimental data are shown for comparison. The error bars for the simulated values, calculated with a 95% confidence interval, are within the size of the symbols.

Table 1. Basal Spacing (in Å) of 1-, 2- 3-, and 4-Layer Hydrated Cs−Montmorillonites

hydration state	present simulation results	other simulations	experiments
0W	10.60	10.53[27]	11.2[18,23]
		10.60−10.70[31]	
		10.50[36]	
1W	12.60	12.68[27]	12.57[17,18]
		12.68[29]	12.3[23]
		12.7[31]	
		12.7, 12.9[35]	
		12.6−12.7[36]	
		12.22[37]	
2W	16.34	15.74−16.33[27]	
		12.0−12.5[28]	
		15.1[35]	
		16.3[36]	
		14.88[37]	
3W	19.58	18.36[35]	
		17.23[37]	
4W	22.23	22.01[27]	
		21.87[35]	

layer hydrate ($x = 10.0$ in our simulations and 8.0−11.0 for other simulations), 3-layer hydrate ($x = 15.0$ in our simulations and 12.0−15.0 for Kosakowski et al.[35]), and 4-layer hydrate ($x = 19.1$ in our simulations and $x = 20$ in ref 35). The equilibrium values of layer spacing for these multilayer hydrates cannot be determined based on the swelling curve alone (Figure 4). In addition, the calculations of the energetic characteristics of Cs−montmorillonite swelling were used, as discussed in the next subsections. On average, our layer spacing values for these multilayer hydrates are somewhat higher than the ones observed in other simulations, but they are very close to the simulation data that also used the CLAYFF force field.[36] The differences with other simulation data can be attributed to the different force fields used,[27−31,35,36,38] to the slightly different clay composition with no tetrahedral charge,[28,31,35] or the presence of both Na$^+$ and Cs$^+$ counterions in the clay interlayers.[31,35]

In the range from $x = 0$ to $x = 4.5$ (0 to 100 mg$_{water}$/g$_{clay}$) the simulated layer spacings are always very close to the

experimental ones, being just slightly lower[17−19] or slightly higher,[23] depending on the sample. Calvet[18,19] and Mooney et al.[17] performed their measurements for montmorillonite samples having no tetrahedral charge and with total layer charges of 0.78|e| and 0.66|e|, respectively. The composition of the montmorillonite sample used in the more recent experiments of Berend et al.[23] was the closest to ours (the tetrahedral charge of 0.22|e| and octahedral charge of 0.526|e|). This may be the reason why for most of the points our results are closer to the ones of Berend et al.[23] and the small differences may be due to different temperatures used (25 °C in this article and 20 °C for the mentioned experimental works).

Beyond $x = 4.5$ (100 mg$_{water}$/g$_{clay}$) experimental data indicate invariable layer spacings unlike the simulation swelling curves that increase. One has to remember, however, that the experimentally measured water contents include contributions not only from the H$_2$O molecules in clay interlayers but also from the ones adsorbed on the external surfaces of clay particles and from the interparticle pore-space (see, e.g., ref 27). Therefore, when the clay interlayer is stabilized ($x = 4.5$) the additional water molecules will preferably adsorb onto the external surfaces, resulting in no noticeable change in the layer spacing value as seen in the experimental data (Figure 4). Besides, one may also consider that clay swelling occurs through the formation of mixed-layer hydrates so that the observed layer spacing is averaged over the interstratified structure,[115] and this may be different from the calculated layer spacing of the uniformly expanded hydrated clay from the simulations that are only due to interlayer water.

3.2. Hydration Energy. The hydration energies of our Cs−montmorillonite models are presented in Figure 5 together
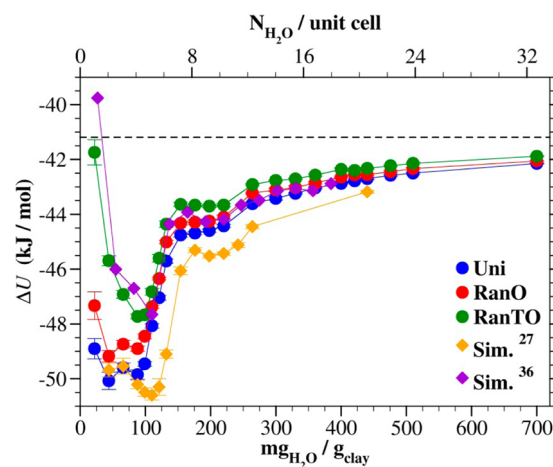
Figure 5. Hydration energy curves for Cs−montmorillonite simulated with the three new clay models and their comparison with previous simulations. The error bars are shown with a 95% confidence interval.

with the results of two other simulations.[27,36] All results exhibit two minima for water contents of $x = 4.5$ (∼100 mg$_{water}$/g$_{clay}$) and $x = 10.0$ (∼220 mg$_{water}$/g$_{clay}$). As expected,[27,107] the hydration energies tend to approach the value of internal energy of bulk water as the water content increases. A comparison between our three clay models shows that the model *Uni* has lower hydration energies compared to the two more disordered models, *RanO* and *RanTO*. However, the energies of *Uni* and *RanO* models are closer to each other than any of these two models with the *RanTO* model. These observations suggest that the variation in the positions of

F

dx.doi.org/10.1021/jp500538z | J. Phys. Chem. C XXXX, XXX, XXX−XXX

octahedral substitutions has a lesser effect on the hydration energy (from *Uni* model to *RanO* in Figure 5) than a similar variation in the tetrahedral sheet (from *RanO* model to *RanTO* model in Figure 5). In addition, one can see that modifying the substitution positions in both octahedral and tetrahedral sheets affects the hydration energy most (from *Uni* model to *RanTO* model) and that the observed differences are very prominent especially at lower water contents before decreasing with increasing hydration. Nevertheless, the compositions of the monolayer and bilayer hydrates are the same for all three models. Further analysis of the swelling energetics based on the calculation of the immersion energy and isosteric heat of adsorption provides additional information for the clear identification of the water contents corresponding of the stable 1W and 2W hydration states and can also help to assign water contents for the hypothetical 3W and 4W hydration states.

The compositions of the monolayer and bilayer hydrates obtained by Liu et al.[36] and by Smith[27] are found, respectively, at water contents of $x = 5$ and $x = 10$ (110 mg$_{water}$/g$_{clay}$ and 220 mg$_{water}$/g$_{clay}$) and $x = 5.5$ and $x = 11$ (120 mg$_{water}$/g$_{clay}$ and 230 mg$_{water}$/g$_{clay}$). From our hydration energies calculations, the stable monolayer and bilayer compositions correspond to water contents of $x = 4.5$ (100 mg$_{water}$/g$_{clay}$) and $x = 10.0$ (220 mg$_{water}$/g$_{clay}$). This means that slightly less water is required in our case to complete the formation of the stable monolayer and bilayer hydrates as compared to the results of Smith.[27] A comparison of the monolayer hydration energies between the three simulations shows that Smith's[27] value is lower than the others, while the energies obtained with the two models labeled *RanO* and *RanTO* are very close to the values of Liu et al.[36] This observation is the same for the bilayer and for higher water contents. This is not surprising since Liu et al.[36] used the same CLAYFF force field (and the SPC model of water) just as we did, but with a set of initial atomic positions[44] that differs from ours. In contrast, Smith[27] has employed the SPC/E water model and Skipper's force field and atomic positions within a rigid clay model.[43,44] Hence the differences/similarities in the initial atomic configuration and force field used can be responsible for the differences/similarities observed between our results and the other simulation results presented.

The small differences observed between Liu et al.'s[36] results and ours show that the swelling energetics can be quite sensitive to variations in the specific clay structure with different locations of substitution sites, even when the total layer charge and the chemical composition remain the same. The observation stands for all three clay models discussed in this work since the observed differences can only be attributed to the differently distributed substitution sites among tetrahedral and octahedral layers because the three models were all treated with the same procedure.

3.3. Immersion Energy and Isosteric Heat of Adsorption.
Figures 6 and 7 show the immersion energies and isosteric heat of adsorption, respectively, for all three models. These two observables provide additional useful information helping to identify the stable hydration states. Apart from the completely dry state corresponding to the first points on the plots, the immersion energies calculated at all other water contents are very similar between the three clay models. Figure 6 allows us to better distinguish the previously observed monolayer and bilayer hydrates through the local minima for $x = 4.5$ (~100 mg$_{water}$/g$_{clay}$) and $x = 10.0$ (~220 mg$_{water}$/g$_{clay}$) for all simulation data presented. Two hypothetical 3-layer and 4-layer hydrates can also be located at water
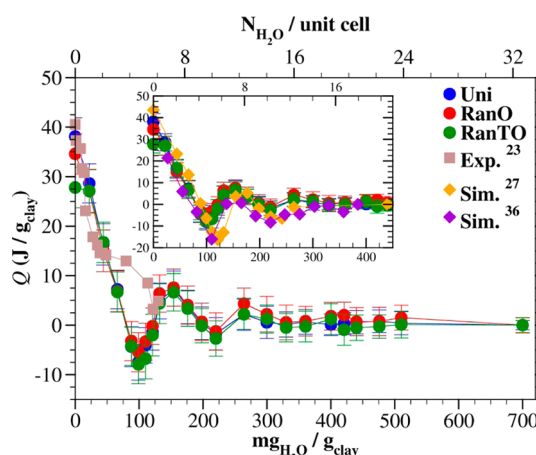
Figure 6. Immersion energy curves simulated for the three new Cs−montmorillonite models and their comparison with experimental data and previous simulations. The error bars are shown with a 95% confidence interval.
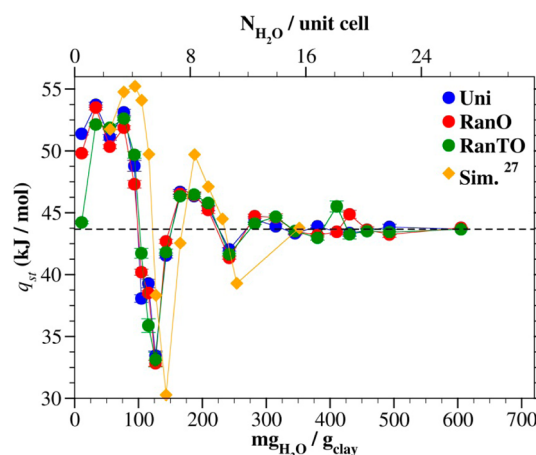
Figure 7. Isosteric heat of adsorption simulated for the three new Cs−montmorillonites models. The error bars are shown with a 95% confidence interval.

contents of 330 mg$_{water}$/g$_{clay}$ ($x = 15.0$) and 420 mg$_{water}$/g$_{clay}$ ($x = 19.1$), that are visible for all three clay models. Though, it is clear on Figure 6 that the immersion energies found beyond 300 mg$_{water}$/g$_{clay}$ do not vary much.

However, the hypothetical 2W hydrates have been earlier observed in the simulation studies,[27,36] and in our work, the hypothetical 3W and 4W hydrates. Cs−montmorillonites are known to form stable monolayer hydrates in water.[115] Our calculations of hydration and immersion energies confirm that the monolayer hydrate is the most stable hydration state. The hydration states beyond 1-layer hydrate (and to some extend 2-layer hydrate) are not observed in experiments under ambient conditions. However, they can be easily probed in the simulations through "forced hydration" of the interlayer spaces by adding more H$_2$O molecules to each interlayer.[27,36] For certain water contents the addition of a small amount of H$_2$O molecules can induce not only the expansion of the clay layers as shown by the increase in layer spacing (Figure 4) but also reorientations and rearrangement of the interlayer water molecules resulting in a small decrease of the total energy of the system and the formation of hypothetical 3W and 4W hydrates (minima in Figure 6 and specified intersections in

G

dx.doi.org/10.1021/jp500538z | J. Phys. Chem. C XXXX, XXX, XXX−XXX
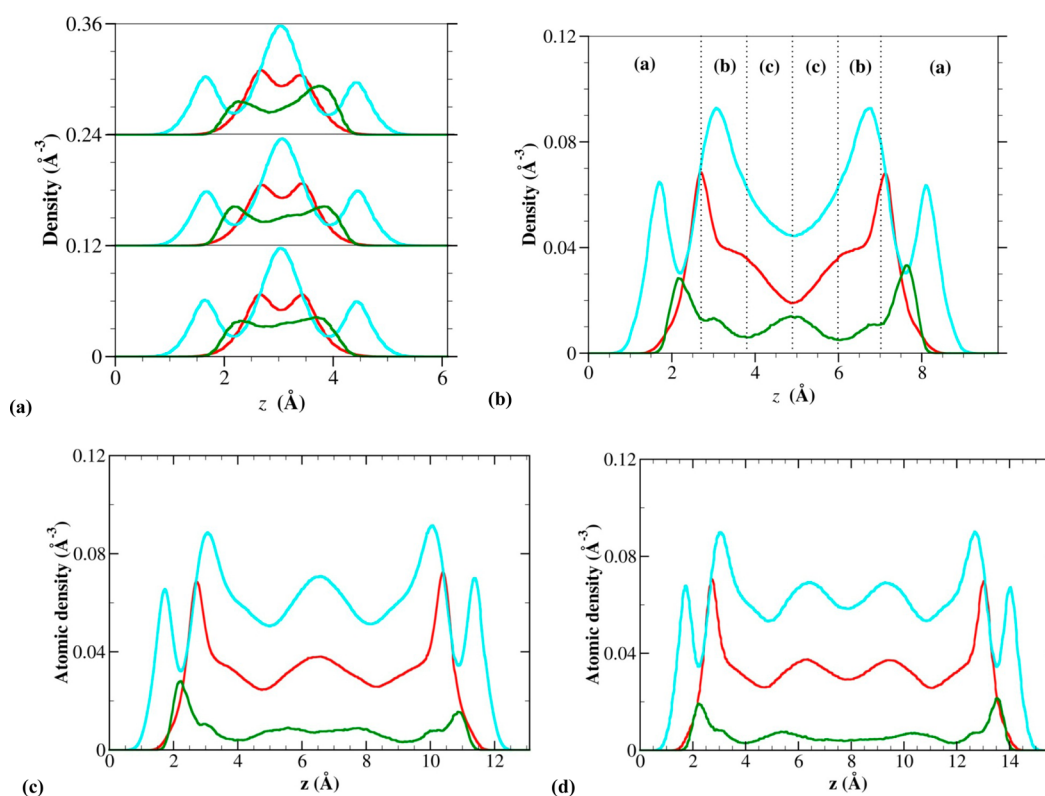
Figure 8. Atomic density distributions along the direction normal to the clay surface, for Cs^+ ions (green), water oxygens (red), and water hydrogens (cyan). The monolayer (a) is shown for three clay models, *RanTO* (topmost), *RanO* (middle), and *Uni* (undermost). The bilayer (b), trilayer (c), and tetralayer (d) hydrates are also shown only for the clay model *RanTO*. Different regions are defined according to Cs^+ ion distributions as shown in panel b.

Figure 7 around 330 and 420 mg_{water}/g_{clay}). Unlike the previous simulation studies,[27,36] these hypothetical 3W and 4W hydrates could be observed in our work because we have systematically probed hydration at water contents up to $x = 32$ (700 mg_{water}/g_{clay}). They are studied here as a sensitive probe to see how much the substitution distribution could affect the formation of successive water layers of the swelling clay.

The calorimetric data of Berend et al.,[23] one of the rare cases when experimental data are available for direct comparison, are displayed in Figure 6 together with our simulation data. These data were digitized from published plots of ref 23 and rescaled to present the immersion enthalpy as a function of water content rather than the original relative humidity variable. In order to be consistent with those data for which bulk water was used as the reference state for immersion enthalpy calculations, and following the work of Liu et al.,[36] the highest water content (700 mg_{water}/g_{clay}, or $x = 32$) was taken as the reference state in eq 6. We also recalculated the immersion energies from Smith[27] using the same consideration (Figure 6).

One can see in Figure 6 that the simulation closely follows experiment[23] for dry and nearly dry clays, but deviates when approaching the monolayer range. The immersion energy decreases close to zero (slightly less than zero for our results and slightly more for the experimental ones) where the stable monolayer hydrate is being formed. As explained by Smith,[27] for a clay that forms monolayer hydrates, the value of the immersion energy would oscillate around the 1-layer hydrate, indicating that small changes in the energy value are associated with external surface hydration. The differences observed between our results and other simulation results[27,36] can be attributed, as before, mostly to the different force field used

and, to some extent, to the location of the substituted sites in the clay layers. An addition source of discrepancy is introduced by the average value of bulk water energy, which is used in deriving the immersion energy as shown by eq 6 and which differs between different water models. In our case this value is equal to -41.2 kJ mol^{-1} (SPC water), while Smith[27] used the value of -41.4 kJ mol^{-1} (SPC/E water), and Liu et al.[36] just used the experimental value of -43.9 kJ mol^{-1} in their calculations.

The immersion energies of the dry clay calculated for our three models all lay in the range 25–40 J/g_{clay} with the *Uni* model being the closest to the experimental value of $\sim$40 J/g_{clay}. The immersion energy value for a dry clay was not provided by Liu et al.[36] After recalculation, Smith's dry clay immersion energy gives $\sim$43 J/g_{clay}, which is closer to experimental value than the value of 60 J/g_{clay} reported in the original paper[27] hwere the reference hydration level did not correspond to the highest water content. This clearly indicates that the most convenient way to evaluate immersion energies from simulations using eq 5 would be to take the highest water content as the reference hydration level, $\langle U(N_0)\rangle$, since it will be closer to bulk water than the 1-layer hydrate used by Smith.[27]

The isosteric heat of adsorption has been introduced and determined before[27] and is calculated here for our three new clay models. It is equivalent to the negative of the differential hydration enthalpy, which, in turn, corresponds to the change in enthalpy of a clay of given water content, per mole of water, upon adsorption of an additional infinitesimal amount of water. The points where the heat of adsorption crosses the bulk vaporization enthalpy of water with negative slope correspond

to stable hydration states.[27] We can then clearly observe the 1-, 2-, 3-, and 4-layer hydrates in Figure 7.

The swelling curves do not show significant differences between the three clay models used, and all of them yield a good prediction of the experimental ones. The swelling energetics clearly shows that immersion energies are only weakly sensitive to the actual distribution of substitutions in the clay sheets, especially at very low water contents. This effect is more pronounced for the hydration energies (Figure 5), but it always weakens as the water content increases.

3.4. Atomic Density Profiles in the Clay Interlayer.

The distribution of interlayer water molecules and Cs^+ ions as a function of their distance from the surface was determined for 1-, 2-, 3-, and 4-layer hydrates (x = 5, 10, 15, and 20, respectively), as shown in Figure 8. Experimental studies of Cs−montmorillonites did not observe the hydration states higher than the monolayer hydrate. Hence, as discussed above, the three other hypothetical hydration states are investigated in this study to see whether the proposed clay models could have different behavior at different hydration states and also to make better comparisons with other simulation studies. The atomic distributions shown in Figure 8 were calculated by averaging over two statistically independent interlayer regions of each model containing the same amounts of water molecules and Cs ions. Cs density in Figure 8 is magnified by a factor of 5 for clarity.

In the monolayer hydrate, for our three clay models, Cs^+ ions and oxygens of H_2O molecules (O_w) have a double-peaked distribution in the interlayer regions with Cs^+ found around 2.3 Å from the clay surface (defined here by the time-averaged positions of the bridging oxygens of the surface siloxane rings (see Figures 2 and 3). The two distinguishable peaks of these distributions indicate the molecular organization near the clay surfaces. Smith[27] and Marry et al.[31] have found that Cs^+ distributes as a single sharp peak in the middle of the interlayer for water content equivalent to a monolayer hydrate, thus showing a lower affinity of Cs^+ to the clay surface than observed in our simulations. Both these previous simulations have used Skipper's rigid clay model and the force field,[43,44] which does not represent the charge delocalization around the substituted sites sufficiently accurately.[58] Moreover, even if Smith[27] used the same amounts of tetrahedral and octahedral substitutions as we did, Marry et al.[31] used a montmorillonite model with only octahedral substitutions. However, it is well-known that the amount of tetrahedral substitutions influences the distribution of ions in montmorillonite interlayers.[32,44] These reasons for the observed disagreements can also be confirmed by the consistency of our results with those of Liu et al.,[36] who had also used the CLAYFF force field in their simulations.

For all three clay models, as we increase the water content to the bilayer hydration state, Cs^+ ion distribution splits into two pairs of symmetric peaks plus a central peak. The highest peak is located around 2.1 Å from the clay surface indicating a tendency for Cs^+ ions to move closer to the clay surface with increased water content and form relatively strong inner-sphere surface complexes, as observed in previous experimental[116,117] and simulation[3,27,31,35,36] studies. These inner-sphere complexes can occupy hexagonal cavities and triangular sites[27,116,118,119] (see Figure 9). Therefore, Cs^+ ions found at ~2.17 Å from the clay surface form inner sphere complexes located in the hexagonal cavities, while inner-sphere complexes formed with the oxygens of the triangular Si or Al sites are indicated by the second lower peak at the clay surface found around 3.1 Å. The
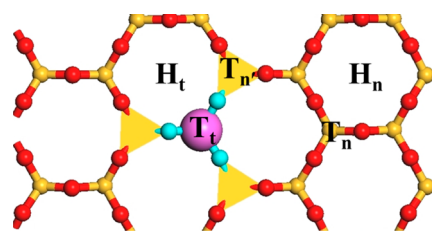
Figure 9. Identification of different binding sites on the clay surface: "normal" hexagonal site without substitution (H_n), hexagonal site adjacent to tetrahedral substitution (H_t), "normal" triangular site without substitution (T_n), substituted triangular site (T_t), and triangular site adjacent to tetrahedral substitution ($T_{n'}$).

third Cs^+ peak is found at ~5.0 Å and represents the outer sphere complexes formed by hydrated cesium ions.

As the water content increases from bilayer to tri- and quad-layer hydrate, the location of the first and second peaks of the Cs^+ density profiles remain about the same, whereas the third peak now shifts to 5.3−5.4 Å from the clay surface, indicating that these Cs^+ ions are not in a relatively stable outer-sphere coordination to the surface but rather in a diffuse aqueous layer.[117] There are no experimental data available for montmorillonite for comparison with these simulations. However, available synchrotron X-ray reflectivity measurements[120] locate Cs^+ around ~2.15 Å from the (001) plane of the muscovite surface. Muscovite also has a 2:1 clay structure with a layer charge almost 3 times higher than montmorillonite and entirely concentrated in the tetrahedral layers.[115] Because of its favorable crystal cleavage properties it is a good model for experimental studies of phenomena occurring at water−mineral interface, unlike montmorillonite.[67] With its high and fully tetrahedral layer charge then, we expect to find Cs^+ ion slightly closer to muscovite surface than to montmorillonite surface, indirectly indicating good agreement of our simulations with available experimental data.

For the hydration states above the monolayer hydrate (x = 10 to 20) and for all three clay models, Cs^+ ions mostly form inner-sphere complexes represented by the peaks at ~2.3 and ~3.1 Å. This is comparable with other simulation data that may have used either different atomic data source or force field and that report Cs−montmorillonite distances of ~2.8,[31] ~3.0,[35] ~2.2−2.5,[36] and ~2.8 Å[3] at water contents higher than the monolayer.

3.5. Atom−Atom Pair Correlation Functions, Lateral Atomic Density Distributions, and Cs^+ Coordination Numbers in the Clay Interlayers.

According to the density profiles presented and discussed above, the clay interlayer space can be divided into 3 regions differing by their representative distance from the surface, where Cs^+ are preferentially located. They are labeled (a), (b), and (c) in Figure 8b. The region (a) (between 0 and ~3 Å from the surface includes Cs^+ ions forming inner-sphere complexes with the hexagonal sites on the clay surface (sites H_n and H_t of Figure 9). The region (b) between ~3 and ~4 Å from the surface is characterized by the Cs^+ ions in the inner-sphere coordination to the triangular sites on the clay surface (sites T_n, $T_{n'}$, and T_t of Figure 9). The region (c) (from ~4 to ~5 Å and more from the surface, depending on the hydration state) comprises cesium ions in the outer-sphere coordination to the surface and/or in the diffuse aqueous layer. The region (a) exists for all the hydration states studied, while the regions (b) and (c) do not develop for the monolayer hydrate and below. Unlike other simulation

Table 2. Positions of the First Maxima (R_{max}) and Minima (R_{min}) of the RDF and the Contribution of Different Oxygen Atoms (O_b, O_{bts}, and O_w) to the First Coordination Shell of Cs^+ Ions in the Interlayer of Hydrated Montmorillonite

hydration state	region	R_{max} (Å)				R_{min} (Å)				N_O				
		O_b	O_{bts}	O_w	O_w (bulk)	O_b	O_{bts}	O_w	O_w (bulk)	O_b	O_{bts}	O_w	O_{tot}	O_w (bulk)
1W	a	3.42	3.15	3.05	3.08	4.30	4.00	4.00	3.96	5.50	0.90	4.92	11.32	8.32
2W	a	3.40	3.15	3.05		4.30	4.00	4.00		4.06	1.37	5.67	11.07	
	b	3.50	3.25	3.05		4.20	4.00	3.98		2.17	0.15	7.62	9.94	
	c			3.07				4.00				8.74	8.74	
3W	a	3.40	3.15	3.05		4.30	4.00	3.95		4.07	1.43	5.66	11.16	
	b	3.50	3.20	3.05		4.20	4.05	3.98		2.29	0.25	7.37	9.91	
	c			3.07				4.00				8.88	8.88	
3W	a	3.40	3.15	3.05		4.30	4.00	3.96		4.14	1.32	5.74	11.20	
	b	3.50	3.20	3.05		4.18	4.05	3.98		2.41	0.22	7.66	10.29	
	c			3.07				4.00				8.95	8.95	

studies,[31,35,36] we decided to carry out a more detailed investigation of the local structure of Cs^+ ions in each of these regions separately.

Quasi-two-dimensional radial distribution functions (RDF) and coordination numbers (CN) for $Cs-O_w$, $Cs-O_b$, and $Cs-O_{bts}$ pairs quantifying the local coordination of Cs^+ ions separately for each of the three regions defined above were determined from monolayer to quad-layer hydrate structures and for each of our three clay models. For a chosen region, only Cs^+ ions located in this region were considered. The results obtained for our three clay models are very similar, with only small differences within the statistical errors of our calculations. Therefore, in the Supporting Information (Figures S3 and S4) we are only showing $Cs-O_b$, $Cs-O_{bts}$, and $Cs-O_w$ RDFs for the most general model *RanTO*. One should note that Cs^+ ions within the region (c) are already too far from the clay surface and only H_2O molecules are forming their first coordination shell. Data in this region are not plotted but are given in Table 2, which provides all quantitative details of the composition of the first coordination shell of Cs^+ in all three interfacial regions (a), (b), and (c) for the four hydration states considered.

The positions of the first maxima on Figures S3, Supporting Information, indicate that Cs^+ ions in the region (a) always bind more strongly to the oxygens coordinating the Al/Si substituted sites, O_{bts} ($Cs-O_{bts}$ distance is 3.12−3.18 Å not far from the $Cs-O_w$ distance slightly less than 3.1 Å), than to the oxygens coordinating nonsubstituted Si sites, O_b ($Cs-O_b$ distance is 3.39−3.43 Å). This observation holds for all hydration states studied and also for the region (b) and can be explained by the local electrostatic inhomogeneity around the substituted site: O_{bts} are slightly more negatively charged than O_b (see Figure 2), as it is reflected by the CLAYFF charge assignment.[58] Unfortunately, similar direct comparisons cannot be made with the results of other simulation studies where the $Cs-O_{clay}$ distributions were calculated without distinguishing the O_b and O_{bts} atom types. However, all previously reported $Cs-O_{clay}$ distances fall in the range between 3.3 and 3.8 Å,[31,35,36] which is consistent with our results. Figure 10 region (c) shows that the $Cs-O_w$ distance is found in the range 3.02−3.10 Å matching well with our calculated bulk value of 3.08 Å and other calculated $Cs-O_w$ distances ranging from 3.0 to 3.21 Å in clay interlayers at different hydration states[13,31,35,36] or in bulk aqueous solution.[121,122] The poor statistical quality of the $Cs-O_{bts}$ radial distribution functions in region (b) is due to the relatively small number of Cs^+ ions located in this region as one can see in Figures 8b−d.
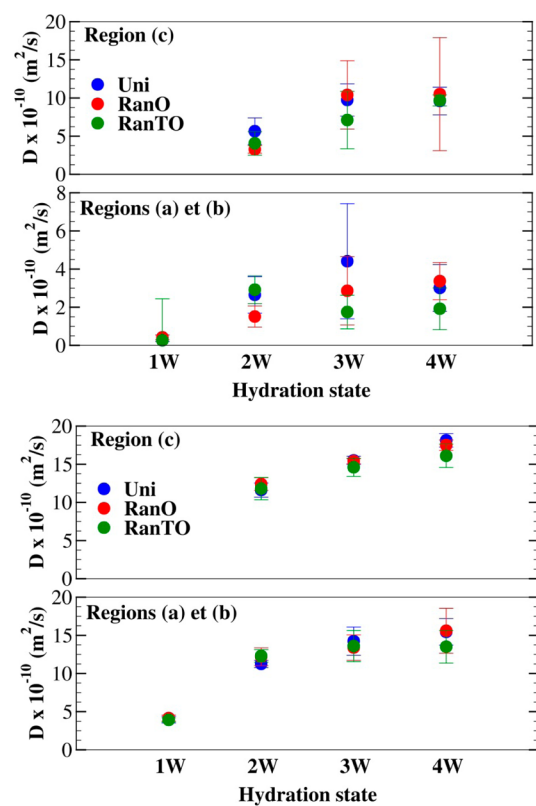
Figure 10. Three dimensional self-diffusion coefficients of Cs^+ ions (a) and water oxygens (b) in the interlayers of hydrated Cs−montmorillonite calculated for the three clay models. The self-diffusion coefficients of Cs^+ and O_{H2O} calculated in this work for a dilute bulk solution are $(21 \pm 4) \times 10^{-10}$ m^2/s and $(31 \pm 1) \times 10^{-10}$ m^2/s, respectively. The error bars are shown with a 95% confidence interval.

The running coordination numbers and the time-averaged populations of various types of oxygen atoms in the first coordination shell of Cs^+ ions in the montmorillonite interlayers are shown in Table 2 (see also Figures S3 and S4 of the Supporting Information). The values in Table 2 were determined using a cutoff value of $R_{min} = 4.0$ Å for all three $Cs-O_b$, $Cs-O_{bts}$, and $Cs-O_w$ pairs. Surprisingly, even though the $Cs-O_{bts}$ distances are shorter, the coordination of Cs^+ with O_b atoms at the surface is much higher. This can be easily explained by the fact that the Al/Si substitutions leading to the presence of O_{bts} atoms are quite rare on the montmorillonite

surface. Only one out of every 60 oxygen atoms are O_{bts} according to the selected clay composition. Therefore, 6 Cs^+ ions that can potentially adsorb on each surface (assuming that the 12 interlayer ions are equally distributed to both clay surfaces) have much higher chances to be coordinated by an O_b atom rather than by an O_{bts} atom.

The number of O_{bts} coordinated to Cs^+ ions in region (a) is equal to 0.90 for the monolayer, 1.37 for the bilayer, 1.43 for the trilayer, and 1.32 for the quad-layer hydrate. In contrast, there are 5.50, 4.06, 4.07, and 4.14 O_b atoms coordinating Cs^+ in the region (a), respectively, for the monolayer, bilayer, trilayer, and quad-layer hydrates. These observations suggest that for the monolayer hydrate ($x = 5$) Cs^+ ions are all found at the hexagonal sites (H_n and H_t in Figure 9). Since the number of H_n sites (no O_{bts} atoms in the hexagonal ring) are larger than H_t sites (2 O_{bts} atoms in the hexagonal ring), this results in a higher $Cs–O_b$ coordination compared to $Cs–O_{bts}$ coordination. As the water content increases to 2-, 3-, and 4-layer hydrates, some of the Cs^+ ions are detached from the hexagonal sites, and most of the remaining Cs^+ ions are located at the H_t sites (Figure 9), so that the averaged local coordination of Cs^+ ions at the clay surface is made of about 4 O_b atoms and more than 1 O_{bts} atom. The charge difference between Al (+1.575$|e|$) and Si (+2.1$|e|$) structural cations in the tetrahedral sheets as well as between the three O_{bts} atoms around the substituting Al atoms (−1.1688$|e|$) and the O_b around the Si atoms (−1.05$|e|$) explain the preference of Cs^+ ions for the H_t sites (see Figures 2 and 9). Even though there are 26/32 H_n sites and only 6/32 H_t sites available on each clay surface for 6 Cs^+ ions, the H_t sites are still electrostatically preferable for Cs^+ sorption.

Cesium ions in region (a) are coordinated to approximately 5 to 6 water molecules bringing the total coordination number close to more than 11. This coordination number is higher by 2 or 3 than in a bulk aqueous solution for which we found a value of 8.32 in agreement with previous findings.[121−124]

In the region (b) and for the different water contents shown, Cs^+ ions are almost always coordinated to 3 surface oxygens with a higher contribution from O_b atoms (more than 2 O_b) compared to O_{bts} atoms (close to 0 O_{bts}). The contributions from the two different types of surface oxygen atoms indicate that Cs^+ ions found in region (b) are located mostly at T_n sites and in some cases at $T_{n'}$ sites (28/32 and 3/32 of all such sites, respectively). The T_t sites only marginally contribute to the Cs-surface coordination within region (b) because the Cs^+ ions preferably adsorbed at the neighboring H_t sites (see Figure 9 and the above discussion) would repel other Cs^+ ions and prevent them from adsorbing at the nearby T_t sites. In addition, there are only 1/32 such tetrahedral sites on each surface. Therefore, the small charge delocalization around the silicon atoms having two O_b and one O_{bts} atoms in their tetrahedra ($T_{n'}$ sites), which are adjacent to the tetrahedrally substituted T_t sites, makes the $T_{n'}$ sites favorable for the adsorption and binding of Cs^+ ions in the region (b).

In this article we combined H_n and H_o sites (Figure 9) into H_n sites[36] unlike Smith[27] who discussed each type of site separately and found that there is no particular correlation between the location of the H_o sites (located above a Mg/Al substitution in the octahedral sheet below) and the adsorption of Cs^+ ions on the clay surface. However, the preferential binding to H_t rather than H_n that we observe in our simulations was also observed in these two previous works.[27,36] One should also note, however, that Liu et al.[36] did not distinguish between different binding sites as a function of their relative distance

from the surface, as proposed by Smith[27] and followed in this work. Nevertheless, Liu et al.[36] have also found a very small contribution from T_t sites compared to H_t sites in the monolayer hydrate, indicating a strong binding preference for the H_t sites as it is was observed by Smith[27] for 1-, 2-, and 4-layer hydrates and in our work for 1-, 2-, 3-, and 4-layer hydrates. Indeed, this is due to a combination of favorable steric and electrostatic reasons: the large area of the hexagonal sites compared to triangular sites, the favorable 6-oxygen coordination compared to only 3-oxygen coordination on the triangular site, the stronger repulsion from Al or Si of the triangular sites compared to the hydroxyl below the hexagonal site,[36] and lower adsorption energy on hexagonal sites compared to triangular sites.[119] No distinction was made between T_n and $T_{n'}$ sites in the previously mentioned papers[27,36] in which both types of sites were termed T_n. Still they found a higher contribution from T_n sites compared to T_t sites as we can now more accurately quantify and explain with our findings.

In this region there are approximately two more H_2O molecules added to the coordination sphere of Cs^+ as compared to region (a) for $x = 10$, 15, and 20 (see Table 2). This indicates that the inner-sphere Cs^+ complexes formed on the triangular sites need additional water molecules in the hydration shell to compensate for the lacking coordination to the surface oxygens, as compared to the region (a).

In the region (c) Cs^+ ions are only coordinated by oxygens of water molecules with coordination numbers varying from 8.74 to 8.95 for $x = 10$ to 20. This is still somewhat higher than the coordination number of Cs^+ in bulk aqueous solutions and can probably be explained by the effect of confinement in the clay interlayer that may induce more densely packed H_2O molecules than in the bulk. Our calculated coordination numbers agree well with previous simulations.[29,31,35]

3.6. Cs^+ Mobility in Montmorillonite Interlayers. The diffusion coefficients of Cs^+ ions and H_2O molecules (O_w) were determined according to eq 10 separately for the regions shown in Figure 8b, and for the entire interlayer space. The regions (a) and (b) were taken together since the structural analysis presented above clearly indicates that Cs^+ forms only inner-sphere surface complexes in both of them. For MSD calculations in each of the defined regions, we considered only atoms belonging to the selected region and those that do not leave this region during the time period between t_0 and t (see eq 10.[3]

The 3D self-diffusion coefficients of Cs^+ ions (Figure 10a) and H_2O (Figure 10b) are plotted as a function of water content for the different regions defined according to Cs^+ distribution in the interlayer space. For different regions, the diffusion coefficients of H_2O always increase with increasing interlayer water content. Adding more water molecules in the interlayer increases the mobility of Cs^+ ions and H_2O molecules at the clay surfaces. The higher number of water molecules compared to Cs^+ ions allows us to have better statistics. This is reflected in the error bars of our calculated diffusion coefficients that are larger for Cs^+ ions than for H_2O molecules.

The mobility of Cs^+ ions in regions (a) and (b) is 2 to 4 times slower compared to region (c), while water diffusion coefficients only slightly vary between these two regions. The attractive effect of the clay surfaces is indeed more important in the case of Cs^+ ions than for water molecules. The calculated diffusion coefficients of water are 5 to 8 times higher than the values obtained for Cs^+ ions in regions (a) and (b), and about 2 times higher in region (c).

Although the model *RanTO* exhibits a somewhat better statistical accuracy than the other two models, present results do not show any systematic trend explaining how the variation in substitution positions affects the mobility of the interlayer species. What can be clearly seen though is that even if the substitution location slightly affects the diffusion coefficient of Cs^+ ions, it almost does not in the case of water molecules.

Table 3 compares the relative diffusion coefficients obtained from our simulations with experimental data and previous

Table 3. Relative Diffusion Coefficients of Cs^+ Ions and H_2O Molecules in the Interlayers of Montmorillonite

	data source	Cs^+	H_2O
1W	simulations		
	present work	0.02–0.03	0.12–0.14
		0.02–0.07[35]	0.10–0.18[35]
		0.05–0.08[31]	0.16–0.21[31]
		0.006[70]	0.04[70]
		0.01[38]	0.16[38]
		0.03[36]	0.16[36]
	experimental data	≤0.008[20,126]	
		≤4 × 10^{-6}[19]	
2W	present work	0.14–0.19	0.38–0.40
		0.18–0.25[35]	0.36–0.39[35]
		0.53[31]	0.42[31]
		0.03[70]	0.18[70]
		0.02[38]	0.42[38]
3W	present work	0.31–0.44	0.48–0.52
		0.30–0.42[35]	0.48–0.54[35]
		0.05[70]	0.29[70]
		0.06[38]	0.69[38]
4W	present work	0.34–0.41	0.52–0.60
		0.37[35]	0.67[35]

simulation results. In most cases, previous simulations provided D_{xyz}, the total diffusion coefficient of the species they calculated. According to eq 11, we then divided these values by the corresponding bulk self-diffusion coefficients provided or mentioned in each of the original papers. In the other cases, the relative diffusion coefficient was already provided, but given in terms of D_{xy}/D_{bulk}. Considering that D_{xy} is almost 3/2 of D_{xyz} we then divided these values by 3/2 to get the data comparable to ours. For the experimental data, we simply divided the various experimental interlayer diffusion coefficients by the bulk experimental values of Cs^+ ions[85] and water.[125]

As discussed above, only the monolayer hydrate was investigated in experiments. There is a very large scatter of experimental values, and our relative diffusion coefficient is 2 to 4 times higher than the maximum value obtained from diffusion experiments in a bentonite at different compaction densities and ionic strengths.[20,126] One possible source of such a discrepancy is that unlike the simulations, which only look at the adsorption and diffusion in the interlayers, in real clay samples significant adsorption can happen at the clay particle edges, further retarding the diffusion of Cs^+ ions in montmorillonite. Indeed, our calculations show very good agreement with other similar simulation data, especially for the monolayer hydrate. The small differences observed increase from 2- to 4-layer hydrates, with our data being always lower than the others. Since we have already minimized the effects of the force used to describe water and ions by using the relative diffusion coefficient, the observed discrepancies between our

simulations and others may come from the presence of both Na^+ and Cs^+ ions in the clay interlayer and the absence of tetrahedral substitution in the clay composition,[31,36,70] or the different force field parameters used for the clay structure.[31,36,38]

4. CONCLUSIONS

We have developed three new models of montmorillonite clay based on different degrees of disorder in the location of Al/Si and Mg/Al isomorphic substitutions in their tetrahedral and octahedral sheets. The models were thoroughly tested in MD simulations of Cs–montmorillonite using the CLAYFF force field to take advantage of its ability to model local charge inhomogeneities around the substituted sites and to investigate how various distributions of these inhomogeneities affect the thermodynamics of clay swelling and the structure and mobility of aqueous species in clay interlayers.

We have demonstrated that the specific localization of substitutions in the TOT layers do not affect the layer spacing at all, but at lower water contents up to 1-layer hydrate, changing the locations of octahedral substitutions in the two TOT layers of montmorillonite can induce a variation of hydration energy from 1 to 2 kJ/mol in absolute values, and similar changes in the tetrahedral sheets can lead to the variation in hydration energy from 1 to 8 kJ/mol in absolute values. However, the calculated values of the immersion energy and the isosteric heat of adsorption demonstrate much less sensitivity to these modifications of the local clay structure.

Detailed investigations of the structure of interlayer Cs^+ ions allowed us to identify and probe four different binding sites on the basal clay surface that are identical for all the clay models studied. The analysis of diffusional dynamics of interlayer species at different distances from the clay surface demonstrates, as expected, that the mobility Cs^+ ions and H_2O molecules increases both with increasing interlayer water content and increasing distance from the clay surface. Only very small differences within the statistical errors of our calculations were observed between the three clay models. Our simulated results are in good agreement with available experimental data on the thermodynamics and structure of Cs–montmorillonite and also consistent with the results of previous simulations.

In summary, we can conclude that the specific localization of isomorphic substitutions in the structure of Cs–montmorillonite has only a minor effect on the thermodynamic, structural, and transport properties of the system, given the same clay composition, the same total layer charge, and the same distribution of this charge between the octahedral and tetrahedral layers of clay. Since clay properties strongly depend on its composition and the nature of interlayer cations, we expect the effects of disorder in the distribution of the layer charge inhomogeneities to be much stronger in the case of the clays with higher total layer charge (higher concentration of substituted sites) and for divalent and trivalent interlayer cations. The MD simulations to quantify these effects are currently in progress and will be reported separately.

■ ASSOCIATED CONTENT

Ⓢ Supporting Information

Additional snapshots illustrating the construction of the new clay models and additional results of their structural analysis. The atomic configurations of the three new montmorillonite

L

dx.doi.org/10.1021/jp500538z | J. Phys. Chem. C XXXX, XXX, XXX–XXX

models are given in separate CIF files. This material is available free of charge via the Internet at http://pubs.acs.org.

■ AUTHOR INFORMATION

Corresponding Author

*(A.G.K.) E-mail: kalinich@subatech.in2p3.fr.

Notes

The authors declare no competing financial interest.

■ REFERENCES

(1) Van Olphen, H. *An Introduction to Clay Colloid Chemistry for Clay Technologists, Geologists, and Soil Scientists*; Wiley: New York, 1977.

(2) Ferrage, E.; Lanson, B.; Sakharov, B. A.; Drits, V. A. Investigation of Smectite Hydration Properties by Modeling Experimental X-ray Diffraction Patterns: Part I. Montmorillonite Hydration Properties. *Am. Mineral.* **2005**, *90*, 1358−1374.

(3) Rotenberg, B.; Marry, V.; Malikova, N.; Turq, P. Molecular Simulation of Aqueous Solutions at Clay Surfaces. *J. Phys.: Condens. Matter* **2010**, *22*, 284114.

(4) Miller, A. W.; Wang, Y. Radionuclide Interaction with Clays in Dilute and Heavily Compacted Systems: A Critical Review. *Environ. Sci. Technol.* **2012**, *46*, 1981−1994.

(5) *ONDRAF/NIRAS Technical Overview of the SAFIR 2 Report*: Safety Assessment and Feasibility Interim Report 2; Belgian Agency for Radioactive Waste and Enriched Fissile Materials: Fleurus, Belgium, 2001.

(6) *NAGRA TECHNICAL REPORT 02-05: Project Opalinius Clay*. Safety Report: Demonstration of Disposal Feasibility for Spent Fuel, Vitrified High-Level Waste and Long-Lived Intermediate-Level Waste (Entsorgungsnachweis); NAGRA: Wettingen, Switzerland, 2002.

(7) Bradbury, M. H.; Baeyens, B. *Near Field Sorption Data Bases for Compacted MX-80 Bentonite for Performance Assessment of a High Level Radioactive Waste Repository in Opalinus Clay Host Rock*; Paul-Scherrer-Institut: Villigen, Switzerland, 2003.

(8) Vieillard, P.; Ramírez, S.; Bouchet, A.; Cassagnabère, A.; Meunier, A.; Jacquot, E. Alteration of the Callovo-Oxfordian Clay from Meuse-Haute Marne Underground Laboratory (France) by Alkaline Solution: II. Modelling of Mineral Reactions. *Appl. Geochem.* **2004**, *19*, 1699−1709.

(9) *ANDRA Dossier 2005: Évaluation de la faisabilité du stockage géologique en formation argile-Synthése*; ANDRA: Châtenay-Malabry, France, 2005.

(10) Altmann, S.; Tournassat, C.; Goutelard, F.; Parneix, J.-C.; Gimmi, T.; Maes, N. Diffusion-Driven Transport in Clayrock Formations. *Appl. Geochem.* **2012**, *27*, 463−478.

(11) Brigatti, M. F.; Galan, E.; Theng, B. K. G. Chapter 2: Structures and Mineralogy of Clay Minerals. In *Developments in Clay Science*; Elsevier: Amsterdam, The Netherlands, 2006.

(12) Onodera, Y.; Iwasaki, T.; Ebina, T.; Hayashi, H.; Torii, K.; Chatterjee, A.; Mimura, H. Effect of Layer Charge on Fixation of Cesium Ions in Smectites. *J. Contam. Hydrol.* **1998**, *35*, 131−140.

(13) Sutton, R.; Sposito, G. Molecular Simulation of Interlayer Structure and Dynamics in 12.4 Å Cs-Smectite Hydrates. *J. Colloid Interface Sci.* **2001**, *237*, 174−184.

(14) Bergaya, F. *Handbook of Clay Science*; Elsevier: Oxford, U.K., 2006.

(15) Pusch, R. *The Microstructure of MX-80 Clay with Respect to Its Bulk Physical Properties under Different Environmental Conditions*; Svensk Kärnbränslehantering AB/Swedish Nuclear Fuel and Waste Management Co.: Stockholm, Sweden, 2001.

(16) Hendricks, S. B.; Nelson, R. A.; Alexander, L. T. Hydration Mechanism of the Clay Mineral Montmorillonite Saturated with Various Cations. *J. Am. Chem. Soc.* **1940**, *62*, 1457−1464.

(17) Mooney, R. W.; Keenan, A. G.; Wood, L. A. Adsorption of Water Vapor by Montmorillonite. II. Effect of Exchangeable Ions and Lattice Swelling as Measured by X-ray Diffraction. *J. Am. Chem. Soc.* **1952**, *74*, 1371−1374.

(18) Calvet, R. Hydration of Montmorillonite and Diffusion of Exchangeable Cations. 1. Hydration of Montmorillonite Saturated by Monovalent Cations. *Ann. Agron.* **1973**, *24*, 77−133.

(19) Calvet, R. Hydration of Montmorillonite and Diffusion of Exchangeable Cations. 2. Diffusion of Exchangeable Cations in Montmorillonite. *Ann. Agron.* **1973**, *24*, 135−217.

(20) Sato, H.; Ashida, T.; Kohara, Y.; Yui, M.; Sasaki, N. Effect of Dry Density on Diffusion of Some Radionuclides in Compacted Sodium Bentonite. *J. Nucl. Sci. Technol.* **1992**, *29*, 873−882.

(21) Sato, T.; Watanabe, T.; Otsuka, R. Effects of Layer Charge, Charge Location, and Energy Change on Expansion Properties of Dioctahedral Smectites. *Clays Clay Miner.* **1992**, *40*, 103−113.

(22) Cornell, R. Adsorption of Cesium on Minerals: A Review. *J. Radioanal. Nucl. Chem.* **1993**, *171*, 483−500.

(23) Berend, I.; Cases, J.-M.; Francois, M.; Uriot, J.-P.; Michot, L.; Masion, A.; Thomas, F. Mechanism of Adsorption and Desorption of Water Vapor by Homoionic Montmorillonites: 2. The Li^+, Na^+, K^+, Rb^+ and Cs^+-Exchanged Forms. *Clays Clay Miner.* **1995**, *43*, 324−336.

(24) Staunton, S.; Roubaud, M. Adsorption of ^{137}Cs on Montmorillonite and Illite; Effect of Charge Compensating Cation, Ionic Strength, Concentration of Cs, K and Fulvic Acid. *Clays Clay Miner.* **1997**, *45*, 251−260.

(25) Kozaki, T.; Sato, H.; Sato, S.; Ohashi, H. Diffusion Mechanism of Cesium Ions in Compacted Montmorillonite. *Eng. Geol.* **1999**, *54*, 223−230.

(26) Gournis, D.; Lappas, A.; Karakassides, M.; Többens, D.; Moukarika, A. A Neutron Diffraction Study of Alkali Cation Migration in Montmorillonites. *Phys. Chem. Miner.* **2008**, *35*, 49−58.

(27) Smith, D. E. Molecular Computer Simulations of the Swelling Properties and Interlayer Structure of Cesium Montmorillonite. *Langmuir* **1998**, *14*, 5959−5967.

(28) Young, D. A.; Smith, D. E. Simulations of Clay Mineral Swelling and Hydration: Dependence upon Interlayer Ion Size and Charge. *J. Phys. Chem. B* **2000**, *104*, 9163−9170.

(29) Sutton, R.; Sposito, G. Molecular Simulation of Interlayer Structure and Dynamics in 12.4-Å Cs-Smectite Hydrates. *J. Colloid Interface Sci.* **2001**, *237*, 174.

(30) Sutton, R.; Sposito, G. Animated molecular dynamics simulations of hydrated caesium-smectite interlayers. *Geochem. Trans.* **2002**, *3*, 73−80.

(31) Marry, V.; Turq, P.; Cartailler, T.; Levesque, D. Microscopic Simulation of Structure and Dynamics of Water and Counterions in a Monohydrated Montmorillonite. *J. Chem. Phys.* **2002**, *117*, 3454−3463.

(32) Marry, V.; Turq, P. Microscopic Simulations of Interlayer Structure and Dynamics in Bihydrated Heteroionic Montmorillonites. *J. Phys. Chem. B* **2003**, *107*, 1832−1839.

(33) Marry, V.; Rotenberg, B.; Turq, P. Structure and Dynamics of Water at a Clay Surface from Molecular Dynamics Simulation. *Phys. Chem. Chem. Phys.* **2008**, *10*, 4802−4802.

(34) Rotenberg, B.; Marry, V.; Dufrêche, J.-F.; Malikova, N.; Giffaut, E.; Turq, P. Modelling Water and Ion Diffusion in Clays: A Multiscale Approach. *C.R. Chim.* **2007**, *10*, 1108−1116.

(35) Kosakowski, G.; Churakov, S. V.; Thoenen, T. Diffusion of Na and Cs in Montmorillonite. *Clays Clay Miner.* **2008**, *56*, 190−206.

(36) Liu, X.; Lu, X.; Wang, R.; Zhou, H. Effects of Layer-Charge Distribution on the Thermodynamic and Microscopic Properties of Cs-Smectite. *Geochim. Cosmochim. Acta* **2008**, *72*, 1837−1847.

(37) Zheng, Y.; Zaoui, A.; Shahrour, I. A Theoretical Study of Swelling and Shrinking Of Hydrated Wyoming Montmorillonite. *Appl. Clay Sci.* **2011**, *51*, 177−181.

(38) Zheng, Y.; Zaoui, A. How Water and Counterions Diffuse into the Hydrated Montmorillonite. *Solid State Ionics* **2011**, *203*, 80−85.

(39) Zheng, Y.; Zaoui, A. Temperature Effects on the Diffusion of Water and Monovalent Counterions in the Hydrated Montmorillonite. *Phys. A* **2013**, *392*, 5994−6001.

(40) Boek, E. S.; Coveney, P. V.; Skipper, N. T. Monte Carlo Molecular Modeling Studies of Hydrated Li-, Na-, and K-Smectites: Understanding the Role of Potassium as a Clay Swelling Inhibitor. *J. Am. Chem. Soc.* **1995**, *117*, 12608−12617.

(41) Boek, E. S.; Coveney, P. V.; Skipper, N. T. Molecular Modeling of Clay Hydration: A Study of Hysteresis Loops in the Swelling Curves of Sodium Montmorillonites. *Langmuir* **1995**, *11*, 4629−4631.

(42) Skipper, N. T.; Refson, K.; McConnell, J. D. C. Computer Simulation of Interlayer Water in 2:1 Clays. *J. Chem. Phys.* **1991**, *94*, 7434−7445.

(43) Skipper, N. T.; Chang, F.-R.; Sposito, G. Monte Carlo Simulation of Interlayer Molecular Structure in Swelling Clay Minerals. 1. Methodology. *Clays Clay Miner.* **1995**, *43*, 285−293.

(44) Skipper, N. T.; Sposito, G.; Chang, F.-R. Monte Carlo Simulation of Interlayer Molecular Structure in Swelling Clay Minerals. 2. Monolayer Hydrates. *Clays Clay Miner.* **1995**, *43*, 294−303.

(45) Skipper, N. T. Computer Simulation of Aqueous Pore Fluids in 2:1 Clay Minerals. *Miner. Mag.* **1998**, *62*, 657−667.

(46) Skipper, N. T.; Lock, P. A.; Titiloye, J. O.; Swenson, J.; Mirza, Z. A.; Howells, W. S.; Fernandez-Alonso, F. The Structure and Dynamics of 2-Dimensional Fluids in Swelling Clays. *Chem. Geol.* **2006**, *230*, 182−196.

(47) Chang, F.-R. C.; Skipper, N. T.; Sposito, G. Computer Simulation of Interlayer Molecular Structure in Sodium Montmorillonite Hydrates. *Langmuir* **1995**, *11*, 2734−2741.

(48) Chang, F.-R. C.; Skipper, N. T.; Sposito, G. Monte Carlo and Molecular Dynamics Simulations of Interfacial Structure in Lithium-Montmorillonite Hydrates. *Langmuir* **1997**, *13*, 2074−2082.

(49) Chang, F.-R. C.; Skipper, N. T.; Sposito, G. Monte Carlo and Molecular Dynamics Simulations of Electrical Double-Layer Structure in Potassium-Montmorillonite Hydrates. *Langmuir* **1998**, *14*, 1201−1207.

(50) Karaborni, S.; Smit, B.; Heidug, W.; Urai, J.; van Oort, E. The Swelling of Clays: Molecular Simulations of the Hydration of Montmorillonite. *Science* **1996**, *271*, 1102−1104.

(51) Chatterjee, A.; Iwasaki, T.; Ebina, T.; Miyamoto, A. A DFT Study on Clay−Cation−Water Interaction in Montmorillonite and Beidellite. *Comput. Mater. Sci.* **1999**, *14*, 119−124.

(52) Chatterjee, A.; Ebina, T.; Onodera, Y.; Mizukami, F. Effect of Exchangeable Cation on the Swelling Property of 2:1 Dioctahedral Smectite: A Periodic First Principle Study. *J. Chem. Phys.* **2004**, *120*, 3414−3424.

(53) Chávez-Páez, M.; de Pablo, L.; de Pablo, J. J. Monte Carlo Simulations of Ca−Montmorillonite Hydrates. *J. Chem. Phys.* **2001**, *114*, 10948−10953.

(54) Chávez-Páez, M.; Van Workum, K.; de Pablo, L.; de Pablo, J. J. Monte Carlo Simulations of Wyoming Sodium Montmorillonite Hydrates. *J. Chem. Phys.* **2001**, *114*, 1405−1413.

(55) Palin, E. J.; Dove, M. T.; Redfern, S. A. T.; Bosenick, A.; Sainz-Diaz, C. I.; Warren, M. C. Computational Study of Tetrahedral Al-Si Ordering in Muscovite. *Phys. Chem. Miner.* **2001**, *28*, 534−544.

(56) Sainz-Diaz, C. I.; Hernández-Laguna, A.; Dove, M. T. Modeling of Dioctahedral 2:1 Phyllosilicates by Means of Transferable Empirical Potentials. *Phys. Chem. Miner.* **2001**, *28*, 130−141.

(57) Sainz-Diaz, C. I.; Timón, V.; Botella, V.; Artacho, E.; Hernández-Laguna, A. Quantum Mechanical Calculations of Dioctahedral 2:1 Phyllosilicates: Effect of Octahedral Cation Distributions in Pyrophyllite, Illite, and Smectite. *Am. Mineral.* **2002**, *87*, 958−965.

(58) Cygan, R. T.; Liang, J.-J.; Kalinichev, A. G. Molecular Models of Hydroxide, Oxyhydroxide, and Clay Phases and the Development of a General Force Field. *J. Phys. Chem. B* **2004**, *108*, 1255−1266.

(59) Cygan, R. T.; Greathouse, J. A.; Heinz, H.; Kalinichev, A. G. Molecular Models and Simulations of Layered Materials. *J. Mater. Chem.* **2009**, *19*, 2470−2481.

(60) Tambach, T. J.; Hensen, E. J. M.; Smit, B. Molecular Simulations of Swelling Clay Minerals. *J. Phys. Chem. B* **2004**, *108*, 7586−7596.

(61) Greathouse, J. A.; Cygan, R. T. Molecular Dynamics Simulation of Uranyl(VI) Adsorption Equilibria onto an External Montmorillonite Surface. *Phys. Chem. Chem. Phys.* **2005**, *7*, 3580−3586.

(62) Greathouse, J. A.; Cygan, R. T. Water Structure and Aqueous Uranyl(VI) Adsorption Equilibria onto External Surfaces of Beidellite, Montmorillonite, and Pyrophyllite: Results from Molecular Simulations. *Environ. Sci. Technol.* **2006**, *40*, 3865−3871.

(63) Wang, J.; Kalinichev, A. G.; Kirkpatrick, R. J.; Cygan, R. T. Structure, Energetics, and Dynamics of Water Adsorbed on the Muscovite (001) Surface: A Molecular Dynamics Simulation. *J. Phys. Chem. B* **2005**, *109*, 15893−15905.

(64) de Pablo, L.; Chávez, M. L.; de Pablo, J. J. Stability of Na-, K-, and Ca-Montmorillonite at High Temperatures and Pressures: A Monte Carlo Simulation. *Langmuir* **2005**, *21*, 10874−10884.

(65) Malikova, N.; Cadène, A.; Marry, V.; Dubois, E.; Turq, P. Diffusion of Water in Clays on the Microscopic Scale: Modeling and Experiment. *J. Phys. Chem. B* **2006**, *110*, 3206−3214.

(66) Sutton, R.; Sposito, G. Molecular Simulation of Humic Substance: Ca-Montmorillonite Complexes. *Geochim. Cosmochim. Acta* **2006**, *70*, 3566−3581.

(67) Meleshyn, A. Aqueous Solution Structure at the Cleaved Mica Surface: Influence of K^+, H_3O^+, and Cs^+ Adsorption. *J. Phys. Chem. C* **2008**, *112*, 20018−20026.

(68) Berghout, A.; Tunega, D.; Zaoui, A. Density Functional Theory (DFT) Study of the Hydration Steps of Na^+/Mg^{2+}/Ca^{2+}/Sr^{2+}/Ba^{2+}-Exchanged Montmorillonites. *Clays Clay Miner.* **2010**, *58*, 174−187.

(69) Botan, A.; Rotenberg, B.; Marry, V.; Turq, P.; Noetinger, B. Carbon Dioxide in Montmorillonite Clay Hydrates: Thermodynamics, Structure, and Transport from Molecular Simulation. *J. Phys. Chem. C* **2010**, *114*, 14962−14969.

(70) Bourg, I. C.; Sposito, G. Connecting the Molecular Scale to the Continuum Scale for Diffusion Processes in Smectite-Rich Porous Media. *Environ. Sci. Technol.* **2010**, *44*, 2085−2091.

(71) Loganathan, N.; Kalinichev, A. G. On the Hydrogen Bonding Structure at the Aqueous Interface of Ammonium-Substituted Mica: A Molecular Dynamics Simulation. *Z. Naturforsch., A: Phys. Sci.* **2013**, *68*, 91−100.

(72) Morrow, C. P.; Yazaydin, A. Ö.; Krishnan, M.; Bowers, G. M.; Kalinichev, A. G.; Kirkpatrick, R. J. Structure, Energetics, and Dynamics of Smectite Clay Interlayer Hydration: Molecular Dynamics and Metadynamics Investigation of Na-Hectorite. *J. Phys. Chem. C* **2013**, *117*, 5172−5187.

(73) Suter, J. L.; Coveney, P. V.; Greenwell, H. C.; Thyveetil, M.-A. Large-Scale Molecular Dynamics Study of Montmorillonite Clay: Emergence of Undulatory Fluctuations and Determination of Material Properties. *J. Phys. Chem. C* **2007**, *111*, 8248−8259.

(74) Okumura, M.; Nakamura, H.; Machida, M. Mechanism of Strong Affinity of Clay Minerals to Radioactive Cesium: First-Principles Calculation Study for Adsorption of Cesium at Frayed Edge Sites in Muscovite. *J. Phys. Soc. Jpn.* **2013**, *82*, 033802.

(75) Hirano, M.; Yonomoto, T.; Ishigaki, M.; Watanabe, N.; Maruyama, Y.; Sibamoto, Y.; Watanabe, T.; Moriyama, K. Insights from review and analysis of the Fukushima Dai-ichi accident. *J. Nucl. Sci. Technol.* **2012**, *49*, 1−17.

(76) Katata, G.; Terada, H.; Nagai, H.; Chino, M. Numerical Reconstruction of High Dose Rate Zones due to the Fukushima Dai-

ichi Nuclear Power Plant Accident. *J. Environ. Radioact.* **2012**, *111*, 2−12.

(77) Ohno, T.; Muramatsu, Y.; Miura, Y.; Oda, K.; Inagawa, N.; Ogawa, H.; Yamazaki, A.; Toyama, C.; Sato, M. Depth Profiles of Radioactive Cesium and Iodine Released from the Fukushima Daiichi Nuclear Power Plant in Different Agricultural Fields and Forests. *Geochem. J.* **2012**, *46*, 287−295.

(78) Oura, Y.; Ebihara, M. Radioactivity Concentrations of ^{131}I, [134]Cs and ^{137}Cs in River Water in the Greater Tokyo Metropolitan Area after the Fukushima Daiichi Nuclear Power Plant Accident. *Geochem. J.* **2012**, *46*, 303−309.

(79) Kobayashi, T.; Nagai, H.; Chino, M.; Kawamura, H. Source Term Estimation of Atmospheric Release due to the Fukushima Daiichi Nuclear Power Plant Accident by Atmospheric and Oceanic Dispersion Simulations. *J. Nucl. Sci. Technol.* **2013**, *50*, 255−264.

(80) Chino, M.; Nakayama, H.; Nagai, H.; Terada, H.; Katata, G.; Yamazawa, H. Preliminary Estimation of Release Amounts of ^{131}I and [137]Cs Accidentally Discharged from the Fukushima Daiichi Nuclear Power Plant into the Atmosphere. *J. Nucl. Sci. Technol.* **2011**, *48*, 1129−1134.

(81) Yoshida, N.; Kanda, J. Tracking the Fukushima Radionuclides. *Science* **2012**, *336*, 1115−1116.

(82) Yoshida, N.; Takahashi, Y. Land-Surface Contamination by Radionuclides from the Fukushima Daiichi Nuclear Power Plant Accident. *Elements* **2012**, *8*, 201−206.

(83) ANDRA. *Inventaire National des matières et déchets radioactifs: Catalogue descriptif des familles*, 2012.

(84) Chaltikyan, V.; Papoyan, A.; Oshita, H.; Shiotani, H.; Ono, K.; Ishikawa, M.; Ozawa, M. Perspectives of Laser-Chemical Isotope Separation of a Long-Lived Fission Product: [135]Cesium. *J. Radioanal. Nucl. Chem.* **2009**, *280*, 343−352.

(85) Flury, M.; Gimmi, T. F. Solute Diffusion. In *Methods of Soil Analysis Part 4: Physical Methods*; Dane, J. H., Topp, G.C., Eds.; Soil Science Society of America: Madison, WI, 2002; pp 1323−1351.

(86) Yasunari, T. J.; Stohl, A.; Hayano, R. S.; Burkhart, J. F.; Eckhardt, S.; Yasunari, T. Cesium-137 Deposition and Contamination of Japanese Soils Due to the Fukushima Nuclear Accident. *Proc. Natl. Acad. Sci. U.S.A.* **2011**, *108*, 19530−19534.

(87) Cuadros, J.; Sainz-Diaz, C. I.; Ramirez, R.; Hernandez-Laguna, A. Analysis of Fe Segregation in the Octahedral Sheet of Bentonitic Illite-Smectite by Means of FTIR, ^{27}Al MAS NMR and Reverse Monte Carlo Simulations. *Am. J. Sci.* **1999**, *299*, 289−308.

(88) Vantelon, D.; Pelletier, M.; Michot, L. J.; Barres, O.; Thomas, F. Fe, Mg and Al Distribution in the Octahedral Sheet of Montmorillonites. An Infrared Study in the OH-Bending Region. *Clay Miner.* **2001**, *36*, 369−379.

(89) Vantelon, D.; Montarges-Pelletier, E.; Michot, L. J.; Briois, V.; Pelletier, M.; Thomas, F. Iron Distribution in the Octahedral Sheet of Dioctahedral Smectites. An Fe K-Edge X-ray Absorption Spectroscopy Study. *Phys. Chem. Miner.* **2003**, *30*, 44−53.

(90) Herrero, C. P.; Sanz, J.; Serratosa, J. M. The Electrostatic Energy of Micas as a Function of Si, Al Tetrahedral Ordering. *J. Phys. C: Solid State Phys.* **1986**, *19*, 4169−4181.

(91) Herrero, C. P.; Gregorkiewitz, M.; Sanz, J.; Serratosa, J. M. ^{29}Si MAS-NMR Spectroscopy of Mica-Type Silicates: Observed and Predicted Distribution of Tetrahedral Al-Si. *Phys. Chem. Miner.* **1986**, *15*, 84−90.

(92) Vinograd, V. L. Substitution of [4]Al in Layer Silicates: Calculation of the Al-Si Configurational Entropy According to ^{29}Si NMR Spectra. *Phys. Chem. Miner.* **1995**, *22*, 87−98.

(93) Lee, J. H.; Guggenheim, S. Single Crystal X-ray Refinement of Pyrophyllite-1Zc. *Am. Mineral.* **1981**, *66*, 350−357.

(94) Loewenstein, W. The Distribution of Aluminum in the Tetrahedra of Silicates and Aluminates. *Am. Mineral.* **1954**, *39*, 92−96.

(95) Kalinichev, A. G.; Kirkpatrick, R. J. Molecular Dynamics Modeling of Chloride Binding to the Surfaces of Calcium Hydroxide, Hydrated Calcium Aluminate, and Calcium Silicate Phases. *Chem. Mater.* **2002**, *14*, 3539−3549.

(96) Kirkpatrick, R. J.; Kalinichev, A. G.; Hou, X.; Struble, L. Experimental and Molecular Dynamics Modeling Studies of Interlayer Swelling: Water Incorporation in Kanemite and ASR Gel. *Mater. Struct.* **2005**, *38*, 449−458.

(97) Kumar, P. P.; Kalinichev, A. G.; Kirkpatrick, R. J. Molecular Dynamics Simulation of the Energetics and Structure of Layered Double Hydroxides Intercalated with Carboxylic Acids. *J. Phys. Chem. C* **2007**, *111*, 13517−13523.

(98) Kalinichev, A. G.; Kumar, P. P.; Kirkpatrick, R. J. Molecular Dynamics Computer Simulations of the Effects of Hydrogen Bonding on the Properties of Layered Double Hydroxides Intercalated with Organic Acids. *Philos. Mag.* **2010**, *90*, 2475−2488.

(99) Kerisit, S.; Liu, C.; Ilton, E. S. Molecular Dynamics Simulations of the Orthoclase (0 0 1)- and (0 1 0)-Water Interfaces. *Geochim. Cosmochim. Acta* **2008**, *72*, 1481−1497.

(100) Liu, X.-D.; Lu, X.-C. A Thermodynamic Understanding of Clay-Swelling Inhibition by Potassium Ions. *Angew. Chem., Int. Ed.* **2006**, *45*, 6300−6303.

(101) Liu, T.; Tian, X.-F.; Zhao, Y.; Gao, T. Swelling of K^+, Na^+ and Ca^{2+}-Montmorillonites and Hydration of Interlayer Cations: A Molecular Dynamics Simulation. *Chin. Phys. B* **2010**, *19*, 109101.

(102) Malani, A.; Ayappa, K. G.; Murad, S. Influence of Hydrophilic Surface Specificity on the Structural Properties of Confined Water. *J. Phys. Chem. B* **2009**, *113*, 13825−13839.

(103) Ferrage, E.; Sakharov, B. A.; Michot, L. J.; Delville, A.; Bauer, A.; Lanson, B.; Grangeon, S.; Frapper, G.; Jiménez-Ruiz, M.; Cuello, G. J. Hydration Properties and Interlayer Organization of Water and Ions in Synthetic Na-Smectite with Tetrahedral Layer Charge. Part 2. Toward a Precise Coupling between Molecular Simulations and Diffraction Data. *J. Phys. Chem. C* **2011**, *115*, 1867−1881.

(104) Argyris, D.; Ho, T.; Cole, D. R.; Striolo, A. Molecular Dynamics Studies of Interfacial Water at the Alumina Surface. *J. Phys. Chem. C* **2011**, *115*, 2038−2046.

(105) Ho, T. A.; Argyris, D.; Papavassiliou, D. V.; Striolo, A.; Lee, L. L.; Cole, D. R. Interfacial Water on Crystalline Silica: A Comparative Molecular Dynamics Simulation Study. *Mol. Simul.* **2011**, *37*, 172−195.

(106) Wander, M. C. F.; Clark, A. E. Structural and Dielectric Properties of Quartz−Water Interfaces. *J. Phys. Chem. C* **2008**, *112*, 19986−19994.

(107) Wang, J.; Kalinichev, A. G.; Kirkpatrick, R. J.; Hou, X. Molecular Modeling of the Structure and Energetics of Hydrotalcite Hydration. *Chem. Mater.* **2001**, *13*, 145−150.

(108) Wang, J.; Kalinichev, A. G.; Kirkpatrick, R. J. Structure and Decompression Melting of a Novel, High-Pressure Nanoconfined 2-D Ice. *J. Phys. Chem. B* **2005**, *109*, 14308−14313.

(109) Wang, J.; Kalinichev, A. G.; Kirkpatrick, R. J. Effects of Substrate Structure and Composition on the Structure, Dynamics, and Energetics of Water at Mineral Surfaces: A Molecular Dynamics Modeling Study. *Geochim. Cosmochim. Acta* **2006**, *70*, 562−582.

(110) Wang, J.; Kalinichev, A. G.; Kirkpatrick, R. J. Asymmetric Hydrogen Bonding and Orientational Ordering of Water at Hydrophobic and Hydrophilic Surfaces: A Comparison of Water/Vapor, Water/Talc, and Water/Mica Interfaces. *J. Phys. Chem. C* **2009**, *113*, 11077−11085.

(111) Berendsen, H.; Postma, J.; van Gunsteren, W.; Hermans, J. Interaction Models for Water in Relation to Protein Hydration. In *Intermolecular Forces*; Pullman, B., Ed.; Reidel: Dordrecht, The Netherlands, 1981; pp 331−342.

(112) Flyvbjerg, H.; Petersen, H. G. Error Estimates on Averages of Correlated Data. *J. Chem. Phys.* **1989**, *91*, 461−466.

(113) Plimpton, S. Fast Parallel Algorithms for Short-Range Molecular Dynamics. *J. Comput. Phys.* **1995**, *117*, 1−19.

(114) Allen, M. P.; Tildesley, D. J. *Computer Simulations of Liquids*; Clarendon Press: Oxford, U.K., 1987.

(115) Brindley, G. W.; Brown, G. *Crystal Structures of Clay Minerals and Their X-ray Identification*; Mineralogical Society: New York, 1980.

(116) Kim, Y.; Kirkpatrick, R. J. ^{23}Na and [133]Cs NMR Study of Cation Adsorption on Mineral Surfaces: Local Environments,

Dynamics, and Effects of Mixed Cations. *Geochim. Cosmochim. Acta* **1997**, *61*, 5199−5208.

(117) Bostick, B. C.; Vairavamurthy, M. A.; Karthikeyan, K. G.; Chorover, J. Cesium Adsorption on Clay Minerals: An EXAFS Spectroscopic Investigation. *Environ. Sci. Technol.* **2002**, *36*, 2670−2676.

(118) Weiss, C. A.; Kirkpatrick, R. J.; Altaner, S. P. Variations in Interlayer Cation Sites of Clay Minerals as Studied by ^{133}Cs MAS Nuclear Magnetic Resonance Spectroscopy. *Am. Mineral.* **1990**, *75*, 970−982.

(119) Ebina, T.; Iwasaki, T.; Onodera, Y.; Chatterjee, A. A Comparative Study of DFT and XPS with Reference to the Adsorption of Caesium Ions in Smectites. *Comput. Mater. Sci.* **1999**, *14*, 254−260.

(120) Schlegel, M. L.; Nagy, K. L.; Fenter, P.; Cheng, L.; Sturchio, N. C.; Jacobsen, S. D. Cation Sorption on the Muscovite (0 0 1) Surface in Chloride Solutions Using High-Resolution X-ray Reflectivity. *Geochim. Cosmochim. Acta* **2006**, *70*, 3549−3565.

(121) Schwenk, C. F.; Hofer, T. S.; Rode, B. M. Structure Breaking" Effect of Hydrated Cs$^+$. *J. Phys. Chem. A* **2004**, *108*, 1509−1514.

(122) Xu, X.; Kalinichev, A. G.; Kirkpatrick, R. J. ^{133}Cs and ^{35}Cl NMR Spectroscopy and Molecular Dynamics Modeling of Cs$^+$ and Cl$^-$ Complexation with Natural Organic Matter. *Geochim. Cosmochim. Acta* **2006**, *70*, 4319−4331.

(123) Novikov, A. G.; Rodnikova, M. N.; Savostin, V. V.; Sobolev, O. V. The Study of Hydration Effects in Aqueous Solutions of LiCl and CsCl by Inelastic Neutron Scattering. *J. Mol. Liq.* **1999**, *82*, 83−104.

(124) Du, H.; Rasaiah, J. C.; Miller, J. D. Structural and Dynamic Properties of Concentrated Alkali Halide Solutions: A Molecular Dynamics Simulation Study. *J. Phys. Chem. B* **2007**, *111*, 209−217.

(125) Mills, R. Self-Diffusion in Normal and Heavy Water in the Range 1−45°C. *J. Phys. Chem.* **1973**, *77*, 685−688.

(126) Molera, M.; Eriksen, T. Diffusion of ^{22}Na$^+$, ^{85}Sr^{2+}, ^{134}Cs$^+$ and ^{57}Co^{2+} in Bentonite Clay Compacted to Different Densities: Experiments and Modeling. *Radiochim. Acta* **2002**, *90*, 753−760.